FOREIGN
BROADCAST
INFORMATION
SERVICE

JPRS Report

Science & Technology

Japan

10TH ELECTRONIC MATERIALS
SUBCOMMITTEE SEMINAR

SCIENCE & TECHNOLOGY
JAPAN

10TH ELECTRONIC MATERIALS SUBCOMMITTEE SEMINAR

[Selected papers from the 10th Electronic Materials Subcommittee Seminar on Synthesis and Applications of Ferroelectric and Piezoelectric Thin Film Ceramics, held 30-31 Jan 92 in Tokyo, sponsored by the Ceramics Society of Japan]

CONTENTS

Application of Ferroelectric Thin Films in ICs

[Article by Tadashi Shiosaki, Department of Electronics, Faculty of Engineering, Kyoto University]

[Excerpts] Introduction

At the IEDM in December 1987 and at the ISSCC in February 1988, Chrysalis and Ramtron of the United States announced 512-bit and 256-bit nonvolatile memories using PZT ($Pb_{1-x}Zr_xTiO_3$) ferroelectric thin films.[1,2] Since then, research into ferroelectric thin films and paraelectric films with high dielectric constants has become active[3-10] with a view to their use in IC memories. Research to utilize the reversal of spontaneous polarization of ferroelectric substances in memory devices started in the 1950's using bulk single crystals and ceramic materials,[11] and research in the 1970's mainly involved the use of field effect transistors (FETs) in metal-oxide semiconductor (MOS) gate films,[12-16] but nothing practical emerged from the research in those days. The reason why research into the application of ferroelectric thin films in nonvolatile memory devices has become active again in spite of this is that problems including the discriminating thresholds, voltage values, operating speeds, and reliability have become possible to solve by forming individual memory cells using FET transistor switches of the same form as widely mass-produced very-high-integration DRAMs and ferroelectric thin film capacitors. Progress in thin film technology after the 70s has made it possible to obtain thin films with high quality.

Principle of Nonvolatile Memory Using Ferroelectric Thin Film

A ferroelectric substance has spontaneous polarization, and is defined as a material offering the possibility of reversing spontaneous polarization by an external electric field. Many oxide ferroelectric substances are of the Perovskite type, lithium niobate type, or tungsten bronze type. Figure 1 shows the crystal structure of a Perovskite type material. Taking barium titanate as an example, it has a cubic crystal system at above the Curie temperature which is 120°C and the centers of gravity of the positive and negative charges are coincident. However, at room temperature, the ions displace relatively as shown in Figure 2, and the valence electrons also change their configuration
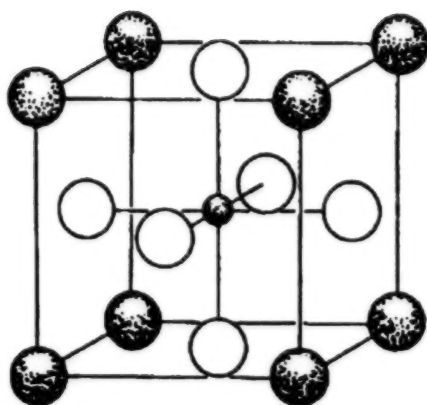
A ⬤ (Ba) ◯ ◯ (O) B ⬤ (Ti)

Figure 1. Structure of
Perovskite Type Crystal

Figure 2. Ionic Configuration of
Barium Titanate at Room Tempera-
ture (Schematic diagram of rec-
tangular surface of cubic crystal
system)

so that permanent electric dipole moment $\Sigma q_i l_i$ (C·m) is generated within the unit lattice. In case displacements with the same directions and sizes as those shown in Figure 2 occur in all crystals, the spontaneous polarization P_s is defined as the permanent electric dipole moment per unit volume, so the size of P_s is equal to $\Sigma q_i l_i N$ (C/m^3) assuming that the volume of the unit tetragonal lattice is V. The orientation of the spontaneous polarization can be aligned with the direction of the external electrical field applied to it. In single crystals as they were fabricated or in microcrystals in ceramics or thin film, the orientation of spontaneous polarization is not aligned but is divided into domains just like the magnetic domains in magnetic substances. When an electrical field is applied to a virgin sample in this condition, polarization

P and electrical field E form a hysteresis curve as shown in Figure 3. After the highest voltage has been applied, the polarization is in state A or C when the electrical field is 0, and remanent polarization $-P_r$ or $+P_r$ is maintained. By defining these states as "0" and "1," respectively, it is possible to select whether "0" or "1" is to be written according to the direction of the application of the electrical field. The value of P_r that can be obtained here is around 10 $\mu C/cm^2$. When the directions of the readout pulse voltage (assume that this is in direction +) and the write direction are the same, that is, in state C, charge of (P_{max} − P_r) x Area, corresponding to C → B, flows. When the electric field has the reverse direction, that is, in state B, a charge of (P_{max} + P_r) x Area, corresponding to A → B, flows. Their difference, which is equal to
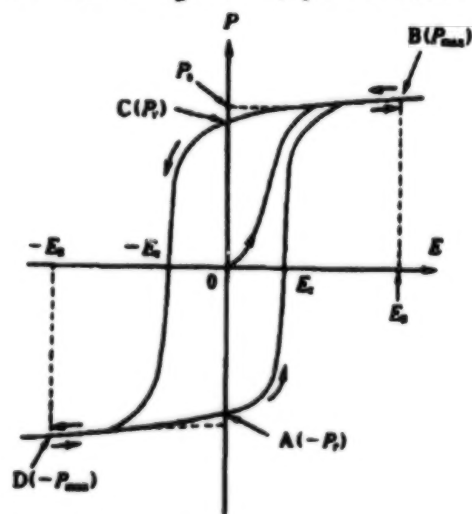

Figure 3. P-E Hysteresis Loop of
Ferroelectric Substance
(E_R indicates readout voltage/
film thickness)

2

$2P_r$ x Area, is the polarization reversal charge. The information can be read by identifying and measuring the quantity of this charge.

Application to Ferroelectric Thin Film Memory

Figure 4 shows the structure of memory announced by Chrysalis. The study of the structure will help understand the advantages, disadvantages and future research themes of ferroelectric thin film memory. The ferroelectric substance seems to have a composition which is close to $Pb_{0.48}Zr_{0.52}TiO_3$. Each cell is basically composed in the same way as in a DRAM, that is, with a transfer gate transistor for switching and a capacitor. The difference from the structure of a
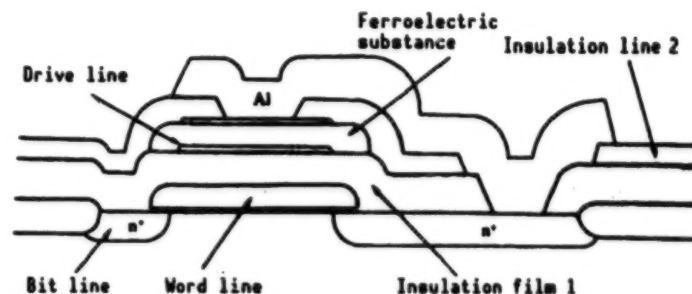

Figure 4. Structure of Nonvolatile Memory Using Ferroelectric Thin Film Announced by Chrysalis[1]

normal DRAM is that the lower electrode of the capacitor is the drive line (DL) and the higher electrode is connected to the transistor. With this structure, PZT thin film elements are fabricated on a platinum thin film in the position shown in Figure 4 because high quality PZT thin film elements cannot be formed on Si or poly-Si, but they are electrically connected to the drain electrode of transistors. With the prototype ferroelectric thin film random access memory (FRAM), each bit is composed of two cells with polarization of the PZT thin film in opposite direction, and the difference between the outputs from the two cells is read out as the signal. According to our estimation, this design is based on the fact that the fluctuations of P_r and P_{max} between all cells due to the variability of the characteristics of PZT thin films in a chip are similar to $P_{max} - P_r$. In other words, the design is based on the fact that discrimination between current accompanied with the reversal charge and current not accompanied with it is difficult in case the characteristics of PZT thin films in a chip are not uniform, but that the characteristic difference is small between two adjacent cells and the discrimination sensitivity can be improved using the difference. The principle itself allows the assignment of one bit per cell like a normal DRAM, but the one-bit-per-two-cells system is adopted because the present current difference (corresponding to the reversal current) is relatively small and that the current variability depending on positions is large.

Table 1 shows a comparison of the characteristics of the present ferroelectric nonvolatile memory (FRAM) with those of other semiconductor memories. The data shows that the FRAM can be an ideal memory device because it has both the high speed of a SRAM or DRAM and the nonvolatility of EEPROM, and that its cell size is basically the same as a DRAM. However, as shown also in Table 1, the rewritable count is not enough at present, making the clarification of the mechanisms of film fatigue and degradation very important research topics.

3

Table 1. Comparison of Characteristics of Nonvolatile Memory Using
Ferroelectric Thin Film (FRAM) and Other Semiconductor Memories

	FRAM	SRAM	DRAM	EEPROM
Read cycle (ns)	25~100	25	150	50~200
Write cycle (ns)	25~100	25	150	10^6
Operating voltage (V)	+5	+5	+5	+5
Write voltage (V)	+5	+5	+5	+12~+21
Radiation resistance (RadSi)	10^6	10^6	$<10^4$	10^4
Power—off hold character- istic (year)	>10 10^{10}	0	0	10~100
Life		∞	∞	10^2~10^5 (write)
Cell area (normalized assuming DRAM area is 1)	1	3	1	2

To avoid film fatigue related to polarization reversal, a memory combining DRAM operation and nonvolatile RAM operation was announced. When the power is ON, this memory device performs the same operation as a normal DRAM by using $(P_{max} - P_r)$ x Area shown in Figure 3 as the stored charge of a DRAM capacitor, and performs nonvolatile RAM operation only when the power is OFF.[17,18] It is reported that, as the spontaneous polarization is not reversed (switched) during DRAM operation because only an electrical field with the same polarity is applied, the film can withstand fatigue up to 10^{13} cycles. In terms of operation, the memory is the same as an NVRAM combining a FRAM and EEPROM, but each ferroelectric thin film can be used in two operations so that the structure is significantly different and the higher degree of integration will be an advantage.

As the information storage of a FRAM is dependent on the direction of spontaneous polarization, it is superior in its resistance to radiation. This resistance to radiation is especially important in space and military applications, and some people think that this characteristic is valuable enough even if the integration does not attain the megabit class.

Application of High-Dielectric Constant Thin Film in DRAMs

High—quality SiO_2 thin films (with a dielectric constant ϵ_r up to 3.8) fabricated by the thermal oxidation of Si have been used as cell capacitors in DRAMs. However, as the degree of integration increases, the necessary SiO_2 film thickness for the required electrostatic capacity has decreased to below 100 Å with DRAMs of 1M or more, almost approaching the limit of thickness reduction. We tried to solve this problem using Si_3N_4 (with ϵ_r up to 7) and fabricating capacitors to increase the capacitor area while keeping the area occupied on the flat surface of the Si substrate small. However, to improve the degree of integration in the future, ferroelectric thin films are essential. Application in DRAMs requires a high dielectric constant or an

important variation of dielectric polarization by the electric field, and does not need the reversal of spontaneous polarization. This may make it possible to utilize the paraelectric phase or $P_{max} - P_r$ which is described above.

Conclusion

Nonvolatile memory using ferroelectric thin film offers the potential to be an ideal semiconductor IC memory, but the devices which have been announced up to now should be regarded as very primitive from the viewpoint of integration and yield. There are still many subjects of research left, including the physical properties, film deposition technology, and microfabrication technology.

Recent research into nonvolatile memory was started in the United States, but we can say that research into ferroelectric thin films themselves is more advanced in Japan. We hope that Japanese semiconductor memory fabrication technology, leading the world, will concern itself with basic research into ferroelectric thin films to give birth to the ideal memory device, the ferroelectric thin film memory.

References

1.   Kinny, W.I, et al., IEDM TECH. DIG., 1987, p 850.

2.   Eaton, S.S., et al., Ibid., 1988, p 1301.

3.   Proc. 1st International Symposium on Integrated Ferroelectrics (ISIF), Colorado Springs, Ferroelectrics.

4.   Proc. 2nd ISIF, San Francisco, Ferroelectrics.

5.   Proc. 3rd ISIF, Colorado Springs, April 1991 (to be published).

6.   ELECTRONICS, February 1988, p 9.

7.   Ibid., August 1989, p 88.

8.   Scott, J.F., et al., SCIENCE, December 1989, p 1400.

9.   Araujo, C.A.P., et al., FERROELECTRICS, Vol 104, 1990, p 24.

10.   NIKKEI MICRODEVICES, May 1989, p 54.

11.   Fazzuzo, E., and Merz, W.J., "Ferroelectricity," North-Holland, Amsterdam, 1967.

12.   Atkins, R.B., FERROELECTRICS, Vol 3, 1972, p 213.

13.   Wu, S.Y., IEEE TRANS. ON ELECTRON DEVICES, Vol Ed-21, 1974, p 499.

14.   Sugibuchi, K., et al., J. APPL. PHYS., Vol 46, 1975, p 2877.

15.   Hamakawa, Y., et al., IEDM TECH. DIG., 1977, p 294.

16.   Matsui, et al., IEICE TECHNICAL REPORT, CPM78, 1978, p 46.

17.   Carrano, J., et al., IEDM TECH. DIG., 1989, p 255.

18.   Mozzani, R., et al., IEEE ELECTRON DEVICES LETTER, Vol 11, 1990, p 454.

19.   ELECTRONIC WORLD NEWS, 4 February 1991.

20.   NIKKEI MICRODEVICES, March 1991.

Synthesis, Application of Pb Ferroelectric Thin Films

[Article by Shigenori Hayashi, Kenji Iijima, and Takashi Hirao, Central Research Laboratories, Matsushita Electric Industrial Co., Ltd.]

[Text] 1. Introduction

Pb oxides such as $PbTiO_3$, PZT, PLT, and PLZT present excellent ferroelectric, pyroelectric, and electrooptical characteristics, and research has been conducted to apply them in infrared sensors and electrooptical elements. Recently, nonvolatile memory devices fabricated by depositing ferroelectric thin films monolithically on Si devices are attracting special attention. As the establishment of thin film deposition technology is very important in their developments, various processes for thin film deposition are being studied, but there are still many problems to be solved in the fabrication of practical high-integration devices that are suitable for practical use, for example high substrate temperature (about 600°C), difficult composition control (particularly the deficit of Pb) and damage due to plasma. In the following, we will first explain the deposition of Pb ferroelectric thin films by the RF magnetron sputtering process and their applications, then describe our attempts with a new thin film deposition process which is more advanced than multitarget sputtering, ion-assisted evaporation, and photo-assisted evaporation.

2. Deposition of Epitaxial Films by Magnetron Sputtering, Their Applications

2.1 PLZT Thin Film and Optical Devices

Since the discovery of PLZT group substances ($(Pb_{1-x/100}La_{x/100})$-$(Zr_{y/100}Ti_{z/100})_{1-x/400}O_3$) with light transmittance and excellent electrooptical phenomena, research into the synthesis of PLZT epitaxial film with excellent properties using sputtering has been conducted with a view to its application in optical devices.

Sintered PLZT is used as the target, and C plane sapphire is used as the substrate because it is suitable for use as an optical device substrate thanks
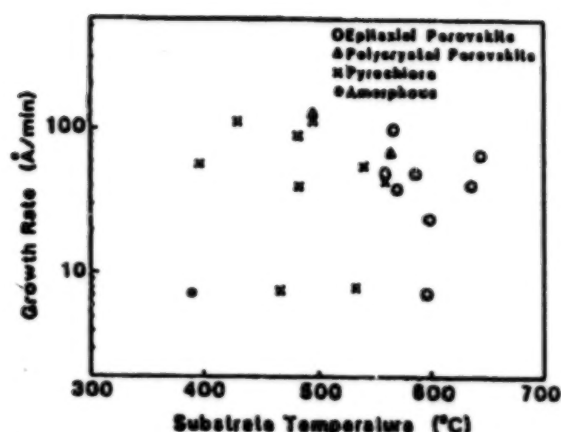
Figure 1. Crystalline Structures of PLZT (28/0/100) Films Deposited at Various Substrate Temperatures and Growth Rate

Figure 2. Schematic Phase Diagram of the Sputtering-Deposited PLZT (0/0/100) (=PbTiO$_3$) Film

to its epitaxial relation with PLZT. Figure 1 shows the crystalline structure of PLZT films deposited in various sputtering conditions. The crystallization characteristics of thin film are dependent mainly on the substrate temperature as shown in Figure 2. To obtain an epitaxial film of the Perovskite phase showing excellent properties, the substrate temperature should be about 600°C. At 550°C or less, thin film obtained has the amorphous or pyrochlore phase. Even if epitaxial state is obtained, the sputtering gas pressure should also be optimized as well as the substrate temperature T$_g$ to obtain the best optical properties.
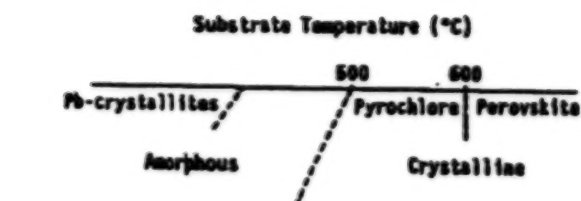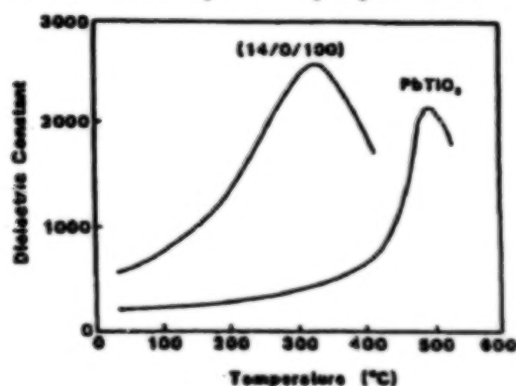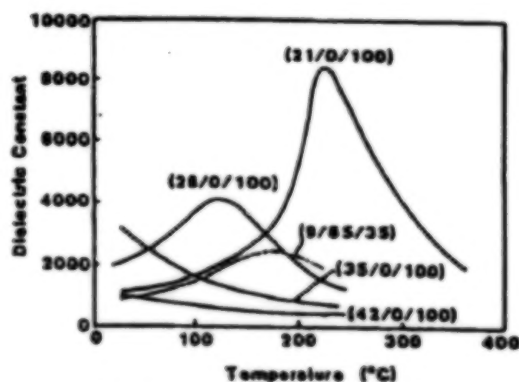

Figure 3. Temperature Dependence of Dielectric Constant for PLZT Epitaxial Thin Films (100 kHz)

Figure 3 shows the temperature dependence of the dielectric constants of PLZT thin films with various compositions deposited under optimized conditions. The figure shows a similar temperature dependence to ceramics, and shows that the Curie temperature T$_c$ decreases as the loadings of La increase. But the dielectric constant of PLZT (9/65/35) which is expected to provide the maximum electrooptical effect is rather low. PLZT containing Zr has poor morphology and its optical characteristics cannot be regarded as satisfactory. Therefore, our development of optical devices was done using PLZT (28/0/100) featuring a high electrooptical effect among the PLTs without any Zr.

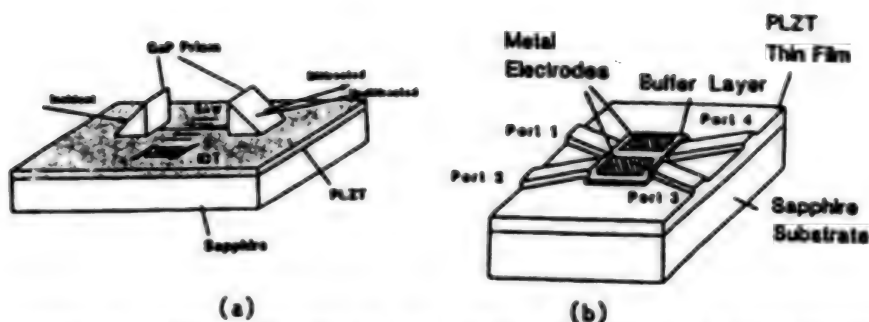Figure 4 shows examples of device applications.

8

Figure 4. Construction of (a) Bragg Acoustooptic Deflector
and (b) Optical TIR (Total Internal Reflection)
Switch Using PLZT Epitaxial Thin Film

2.2 PLT Thin Film and Infrared Sensor

With a large coefficient of pyroelectricity γ and small dielectric constant ϵ_r, thin films of PT ($PbTiO_3$) and PLT with c-axis orientation are expected to be applied in high-sensitivity infrared (IR) sensors.

In the deposition of PLT thin films by magnetron sputtering, we also attempted optimization taking the epitaxy and c-axis orientation into consideration. The target used was also a sintering object, and the substrate used an MgO (100) surface obtained by the growth of Pt thin film with (100) orientation. The c-axis orientation rate is dependent on the gas pressure and growth rate, and a PLT thin film

Figure 5. F_v and F_d as a Function of α

with high c-axis orientation rate can be obtained at a low gas pressure and low growth rate. Also, as shown in Figure 5, the indexes of performance as a pyroelectric material, F_v and F_d, obtained from the measurements of the coefficient of pyroelectricity γ and dielectric constant ϵ_r, improve as the c-axis orientation rate a increases. Taking the PLT composition into consideration, the c-axis orientation of PL10 (= PLZT(10/0/100)) seems to be optimum.

2.3 PZT Thin Film and Ferroelectric Memory

The interest in PZT thin film has also increased since the appearance of nonvolatile memory. The subjects of most research tend to concentrate around the composition PLZT (0/54/46) which present the best characteristics. On this occasion, we show systematic data when the sputtering process is used.

9

Figure 6. Temperature Dependence of the Volume Ratio of Each Film Orientation in the Films for the Sputtered PZT Films on Various Substrates

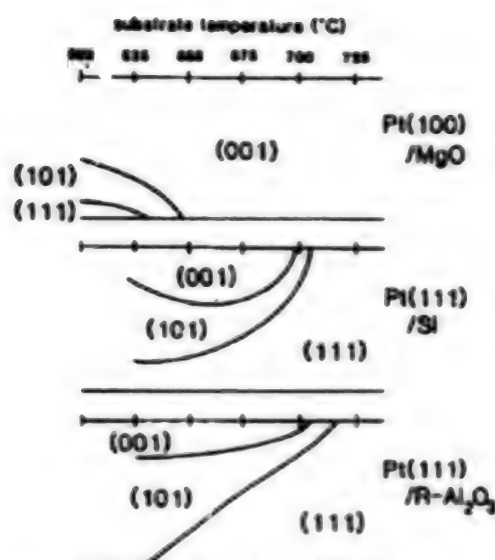Figure 7. P_r and E_c of the PZT Films Deposited on Pt/MgO as a Function Target Composition

Figure 6 shows the substrate temperature T_s dependence of the crystalline structure of PZT (x – 0.20) (– PLZT (0/20/80)) on various substrates. The figure shows that epitaxial film of (001), or c–axis orientation, requires high T_s of more than 650°C, and that the (111) orientation requires T_s to be higher, at 700°C. Figure 7 shows the dependence of remanent polarization P_r and coercive electric field E_c on the composition. The figure shows that "soft" characteristics with large P_r and small E_c, which are suitable for use in memory, are obtained in the rhombohedral phase with x > 0.55.

3. New Thin Film Deposition Processes

This section describes new, advanced thin film deposition processes, which deal with such targets as Pb ferroelectric substances and oxide superconductive materials having similar structures, based on the knowledge of sputtering processes.

3.1 Multitarget Sputtering

The synthesis of PLZT thin films using a single target, described above, has a limit in terms of composition control. Ideally, it is desirable to control the quantity of each element independently. With the multitarget sputtering system shown in Figure 8, PLZT thin film with the desired composition can be obtained by controlling the input power and gas pressure to each of the Pb, La, Zr, and Ti metal targets.
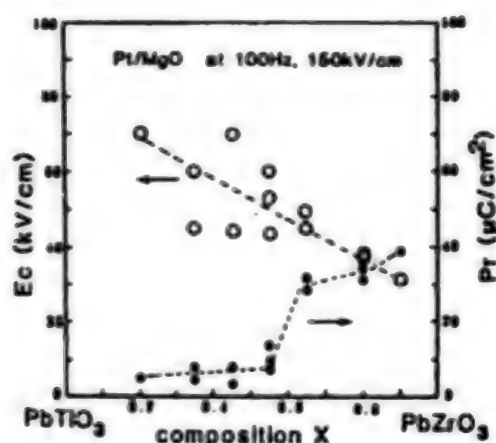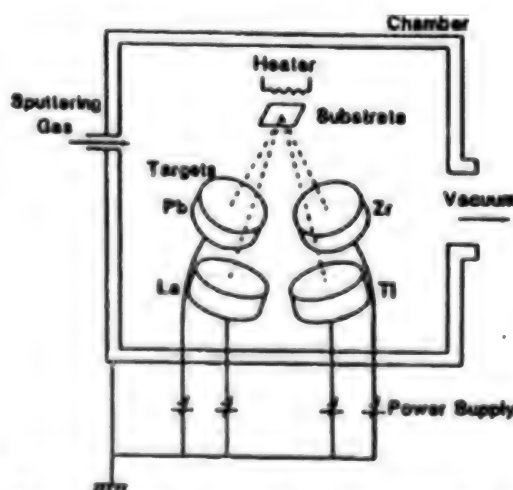

Figure 8. Schematic Illustration of the Multitarget Sputtering System

Another advantage of multitarget sputtering is that it is capable of controlling film composition. It is difficult to obtain high-quality epitaxial film from PLZT containing Zr as described before. However, epitaxial PLZT thin film can be obtained easily by applying the composition control technique in multi-target sputtering and providing a PLT thin film between the PLZT and substrate for use as a buffer layer as shown in Figure 9.

3.2 PbTiO₃ Thin Film Deposition by Means of Ion-Assisted or Photo-Assisted Evaporation

As described before, a substrate temperature T_s of 600°C or more is required to obtain Pb ferroelectric epitaxial film by sputtering. In the following, we will describe the synthesis of $PbTiO_3$ thin film at low temperatures by means of ion- and photo-assisted evaporation techniques.

Figure 9. X-Ray Diffraction Patterns of PLZT Thin Film With and Without Buffer Layer of Graded Composition

Figure 10. Schematic Diagram of the Ion- and Photoassisted Evaporation System (Hybrid ion beam deposition apparatus (A) of the Ion Engineering Center Corp.)

Figure 10 shows the thin film deposition system. Pb and Ti are obtained from metal pellets, and are deposited simultaneously on an MgO(100) substrate by electron beam heating. The oxygen is supplied from a packet-type ion source by bombardment with an oxygen ion beam (accelerating voltage 100 V). An XeCl excimer laser beam is also used. As the composition of the deposited thin film is dependent on the Pb and Ti evaporation rates and the production of PbO or TiO_2 occurs often depending on the condition, this system requires accurate composition control.

Previous processes required a substrate temperature of 600°C or more to obtain $PbTiO_3$ with a Perovskite structure. However, as shown in the X-ray diffraction pattern in Figure 11, this research obtained $PbTiO_3$ with a Perovskite structure at a very low substrate temperature of 450°C by simply applying ion assistance by oxygen ion beam bombardment.

11

Figure 11. (a) XRD Pattern and (b) SEM Micrograph of the
Film Deposited at T_s=450°C by Ion-Assisted
Evaporation (V=100 V, I=40 mA)

Pb and Ti evaporation rates were 2.5 and 0.15 A/s,
respectively.
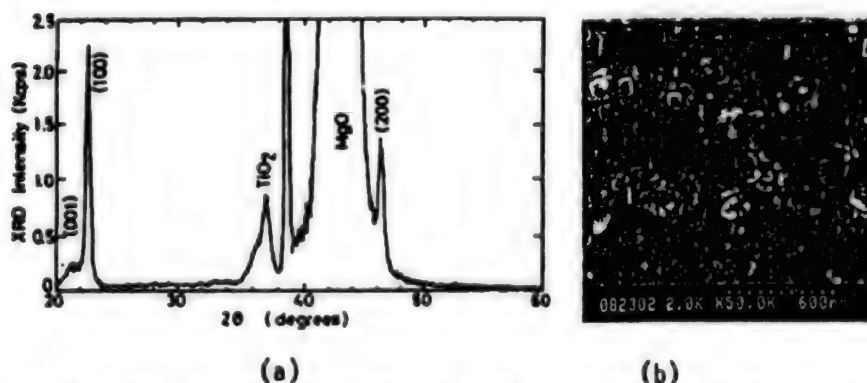
Figure 12. (a) XRD Pattern and (b) SEM Micrograph of the
Film Deposited at Room Temperature by Ion-
and Photoassisted Evaporation (V=200 V, I=80
mA, E=150 mJ/shot, f=100 Hz)

Pb and Ti evaporation rates were 1.0 and 0.25 A/s,
respectively.

If photo assistance by excimer laser irradiation is applied in addition to the
ion assistance, that is, when composite assistance is used, $PbTiO_3$ with a
Perovskite structure can be obtained as shown in the X-ray diffraction pattern
in Figure 12. These results clarified that the composite ion- and photo-
assisted evaporation technique may make it possible to synthesize Pb ferro-
electric thin film at low temperature.

12

4. Conclusion

As described above, the control of the substrate surface during thin film growth and the development of a low-temperature synthesis process are important in the applications of Pb ferroelectric thin films. Our future theme is the optimization of the processes.

5. Acknowledgement

References

1.   Evans, J.T. and Womack, R., IEEE J. SOLID-STATE CIRCUITS, Vol 23, 1988, p 1171.

2.   Iijima, K., Kawashima, S., and Ueda, I,., Proc. 6th Int. Meet. on Ferroelectricity, Kobe, 1985; JPN. J. APPL. PHYS., Vol 24, Suppl. 24-2, 1985,   482.

3.   Wasa, K., Yamazaki, O., Adachi, H., Kawaguchi, T., and Setsune, K., IEEE J. LIGHTWAVE TECH., Vol LT-2, 1984, p 710.

4.   Feldman, C., REV. SCI. INSTRUM., Vol 26, 1955, p 463.

5.   Kusao, K., Wasa, K., and Hayakawa, S., JPN. J. APPL. PHYS., Vol 7, 1968, p 437.

6.   Shintani, Y. and Tada, O., J. APPL. PHYS., Vol 41, 1977, p 2376.

7.   Ishida, M., Matsunami, H., and Tanaka, T., Ibid., Vol 31, 1977, p 433.

8.   Dharmadhikari, V.S. and Grannemann, W.W., Ibid., Vol 53, 1982, p 8988.

9.   Krupanidhi, S.B., Maffei, N., Sayer, M., and El-Assal, K., Ibid., Vol 54, 1983, p 6601.

10.   Iijima, K., Tomita, Y., Takayama, R., and Ueda, I., APPL. PHYS. LETT., Vol 60, 1987, p 361.

11.   Kushida, K. and Takeuchi, H., Ibid., Vol 50, 1987, p 1800.

12.   Haertling, G.H., and Land, C.E., J. AMER. CERAMIC SOC., Vol 54, 1971, p 1.

13.   Haertling, G.H., FERROELECTRICS, Vol 75, 1987, p 25.

14. Adachi, H., Mitsuyu, T, Yamazaki, O, and Wasa, K., J. APPL. PHYS., Vol 60, 1986, p 736.

15. Wasa, K., Adachi, H., Hirochi, K., Setsune, K., Kamada, T., and Kitabatake, M., THIN SOLID FILMS, Vol 163, 1988, p 175.

16. Adachi, H., Mitsuyu, T., Yamazaki, O., and Wasa, K., JAPANESE JOURNAL OF APPLIED PHYSICS, Suppl. 24-2, 1985, p 287.

17. Wasa, K., Yamazaki, O., Adachi, H., Kawaguchi, T., and Setsune, K., IEEE J. LIGHTWAVE TECH., Vol LT-2, 1984, p 710.

18. Iijima, K., Tomita, Y., Takayama, R., and Ueda, I., J. APPL. PHYS., Vol 24, Suppl. 24-3, 1985, p 13.

19. Iijima, K., Takayama, R., Tomita, Y., and Ueda, I., Ibid., Vol 60, 1986, p 2941.

20. Iijima, K., Ueda, I., and Kugimiya, K., JAPANESE JOURNAL OF APPLIED PHYSICS, Vol 30, 1991, p 2149.

21. Adachi, H., Mitsuyu, T., Yamazaki, O., and Wasa, K., Ibid., Suppl. 24-3, 1985, p 13.

22. Hayashi, S., Iijima, K., and Hirao, T., Proc. 8th Meet. on Ferroelectric Materials & Their Applications, Kyoto, 1991; Ibid., Vol 30, 1991, p 2186.

Fabrication, Application of AlN Thin Film by ECR Ion Beam Sputtering

[Article by Hiroshi Okano, Toshiharu Tanaka, Kenichi Shibata, Yusuke Takahashi, Kazuhiko Kuroki, and Shoichi Nakano, Functional Materials Research Center, Sanyo Electric Co., Ltd., and Isao Kiyose, Electronic Components Division, same company]

[Text] 1. Introduction

Following the recent development of mobile communications equipment such as mobile phones, the demand for compact and lightweight devices (filters, duplexers) usable in the microwave band is also increasing. At present, the mainstream of microwave-band devices are dielectric devices using ceramics with a low loss and high dielectric constant, but Sanyo Electric is also developing surface acoustic wave (SAW) devices with the possibility of further size and weight reductions.

The development of SAW devices for use in the microwave band can be approached in two ways: from the aspect of processing such as micro-electrode fabrication, and from the aspect of materials such as the search for materials with high-phase velocities. In this paper, we consider the aspect of materials and introduce the method of fabrication by electron cyclotron resonance (ECR) dual-ion beam sputtering of high-quality thin film of aluminum nitride (AlN), which is attracting attention as a high-phase velocity piezoelectric thin film material, together with its applications in SAW devices.

2. SAW Device Materials

2.1 Required Characteristics

In general, the following points are important for SAW device materials:

> (a) High electromechanical coupling coefficient (0.5 percent or more if possible).
> (b) Small SAW propagation loss (0.2 dB/wavelength).
> (c) Small temperature coefficient of propagation rate (no more than 200 ppm).

Among these, (a) and (b) exert a significant influence on the insertion loss when the device is implemented, and (c) affects the temperature stability.

In addition, to the above, the following two points are very important for use in the microwave band.

 (d) Good surface smoothness.
 (e) High SAW propagation rate.

The center frequency (f_0) of a SAW device can be expressed as a function of the inter-electrode pitch ($\lambda/4$) and SAW velocity (v) as follows:

$$f_0 - v/\lambda$$

As shown by this formula, what is important for the material of SAW devices with higher frequencies is that it is a high-phase velocity material having a smooth surface on which micro-electrode patterns can be fabricated.

Although the micro-electrode pattern fabrication technology is making great progress accompanying the progress of IC technology, electrodes for use in SAW devices are required to have a high aspect ratio and good vibration resistance. As present techniques cannot deal with the submicrowave band; developments of new materials are needed.

From the viewpoint of productivity, the following three additional points are also important.

 (f) High reproducibility in material fabrication.
 (g) No aging in material.
 (h) Possibility of low-cost material fabrication.

2.2 Materials

There may be three kinds of materials for use in high-frequency SAW devices: the single crystals, ceramics, and thin films.

Single-crystal materials can provide a smooth surface, but their phase velocity is determined by the crystal plane and propagation direction. Among materials which currently can provide crystals with a diameter which is large enough for their use in wafer fabrication, the one featuring the highest velocity is $LiTaO_3$ with 36^0Y cut X propagation, which has a velocity of about 4,200 m/sec.[1]

Ceramic materials allow the control of a wide range of piezoelectric characteristics according to their composition and sintering conditions. However, as they are polycrystalline sintered substances, they tend to produce holes which increase the propagation loss and obstruct the fabrication of IDTs. The main ceramic materials being studied now are PZT materials, but they are not suitable for radio frequencies because of their velocities of between 2,000-2,500 m/sec.

16

With thin film materials, the substrate type, film thickness and electrode layout can be set arbitrarily, so that even with the same kind of material or film thickness, the phase velocity, coupling coefficient, and temperature characteristics can be selected with a certain degree of freedom. The surface smoothness is largely dependent on the fabrication method and conditions, but the area of velocity is promising, as there are examples of ZnO deposited on a sapphire substrate[2] and AlN deposited on silicon and sapphire[3] which can achieve velocities of more than 5,000 m/sec.

2.3 Features of AlN, Fabrication Methods

AlN is a compound with a hexagonal crystalline structure belonging to the III-V family, and features high chemical and physical stability.[4] The physical properties of AlN are shown in Table 1. Research is now being conducted actively to use it as an IC package material in place of alumina by making use of its high thermal conductivity.

Table 1. Physical Properties of AlN

Elastic constant $(10^{11}$ N/m$^2)$	C_{11}		C_{13}		C_{33}		C_{44}
	3.45		1.20		3.95		1.18
Dielectric constant $(10^{11}$ F/m$)$	ϵ_{11}				ϵ_{33}		
	8.0				9.5		
Piezoelectric constant (C/m^2)	e_{15}		e_{31}			e_{33}	
	−0.48		−0.58			1.55	
Density $(10^3$ kg/m$^3)$	3.26						

Research into its thin film fabrication is mostly targeted at SAW devices, and almost all film deposition methods have been reported, centered around sputtering[5] and chemical vapor deposition (CVD).[6] The sputtering process allows polycrystalline c-axis orientation film to be obtained easily even on amorphous substrates including glass, and the CVD process allows single crystal films to be obtained on silicon and sapphire substrates although it requires a substrate temperature of 1,000°C or more. Single-crystal thin film is desirable in order to obtain good surface wave characteristics, but the excitation of surface waves is possible even with polycrystalline thin film provided that it has a c-axis orientation, its grain diameter is small enough with respect to the wavelength and its film thickness is optimized. At present, the technology for fabricating high-quality AlN films with good surface wave characteristics and with good reproducibility has not been established using any fabrication method.

3. Fabrication of AlN Thin Film

Aiming at fabrication of high-quality AlN thin films, we are optimizing the fabrication conditions of the dual ion beam sputtering method using electron cyclotron resonance (ECR) which is attracting attention as a highly-efficient ion source.

3.1 Summary of System

Figure 1 shows a schematic diagram of the ER dual ion beam sputtering system. The sputtering ion source is a 5-cm Kaufman ion gun (manufactured by Iontech) and the assisting ion source is an ECR ion gun (manufactured by Ulvac Japan, Ltd.). ECR is a method to obtain high-efficiency plasma by making the frequency of the incident microwave (2.45 GHz) and the rotational motion frequency of electrons in the magnetic field (875 Gauss)[7] coincide.
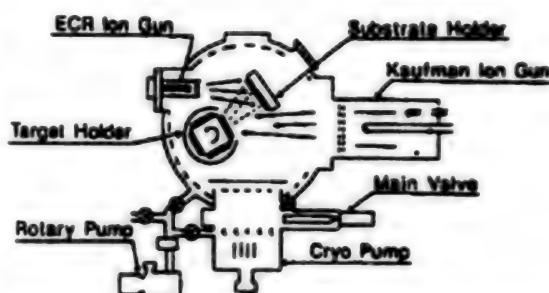

Figure 1. Schematic Diagram of ECR Dual Ion Beam Sputtering System

The dual ion beam sputtering method can deposit high-quality thin films of various compounds thanks to its advantages such as high-vacuum processing, freedom from plasma, and low-temperature processing, and can also synthesize crystal layers which are difficult to fabricate in a state of thermal equilibrium. As this system uses an ECR ion gun which can be assisted with high current density, it is expected to fabricate thin films with even higher quality.

Table 2. AlN Thin Film Deposition Conditions

Target	Al (99.999%)
Substrates	Si(110), sapphire C plane, R plane
Substrate temperatures	R.T.-700°C
N_2 flow rate	8 CCM
Ar flow rate	6 CCM
Operating pressure	1.6×10^{-4} Torr
Kaufman ion gun (sputtering gun)	750 eV, 45 mA
ECR ion gun (assist gun)	100-300 eV, 10 mA
Back pressure	$< 5 \times 10^{-7}$ Torr

18

3.2 Fabrication Method

Table 2 shows the deposition conditions. To make full use of the high-phase velocity of AlN, Si(110) and sapphire C and R planes are used as the substrates. While controlling the Kaufman ion gun so that aluminum reaches the substrate at 32 Å/min, we bombarded a nitrogen ion beam with ECR and examined the substrate temperature, substrate type, the dependence on the nitrogen ion beam energy, and so on. Although there are other important parameters for film deposition such as gas pressure and gas ratio, they are assumed to be constant in our experiments. For the preprocessing of the substrate, it was bombarded with an argon ion beam of 1,000 eV for 10 minutes.

3.3 Results and Considerations

Figure 2 shows the current-versus voltage characteristic of ECR when nitrogen gas is introduced. The current value refers to the value near the leading electrode with a diameter of 5 cm, and does not necessarily coincide with the current value of the nitrogen ion beam when it reaches the substrate. The current values are variable dependent on the microwave power, gas flow, gas pressure, and so on, but our series of experiments assumed a microwave power of 350 W, gas flow of 8 CCM, and a gas pressure (Ar (for sputtering gun) + N_2) of 1.6×10^{-4} Torr.
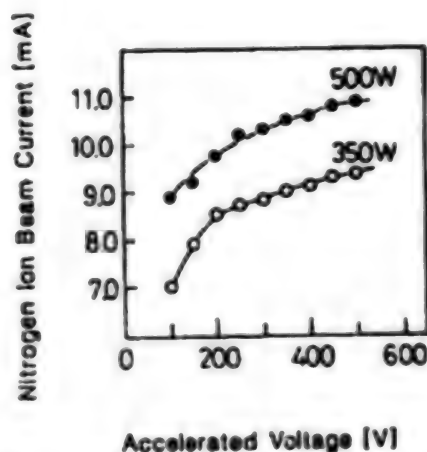

Figure 2. Current Vs. Voltage Characteristic of ECR (Pressure 1.6×10^{-4} Torr, N_2 gas 8 CCM)
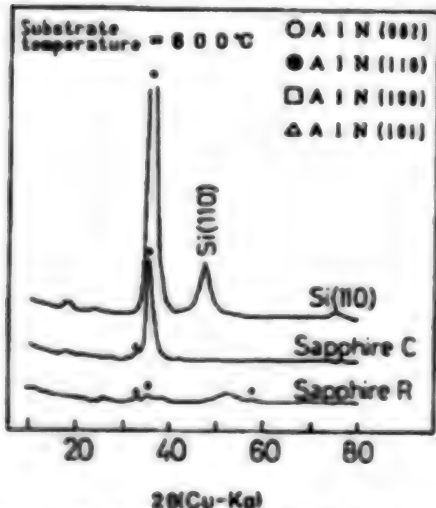

Figure 3. XRD Patterns of AlN Thin Films Deposited on Various Substrates (Substrate temperature 600°C, nitrogen ion beam energy 200 eV)

We first studied the dependence on the substrate type. Figure 3 shows the X-ray diffraction patterns of AlN films deposited on substrates made of Si(110), sapphire C plane and sapphire R plane at a substrate temperature of 600°C and an assisting nitrogen ion beam energy of 200 eV. The AlN films obtained with Si(110) and sapphire C substrates had c-axis orientation, but the AlN film on the sapphire R substrate was polycrystalline. This is because the C plane of hexagonal AlN is the densest plane and also because the condition of the C plane of hexagonal AlN is most suitable for epitaxial growth from the viewpoints of the lattice constants of Si(100) and sapphire C plane. On the other hand, with the sapphire R plane substrate, the (110) plane of hexagonal AlN meets the condition for epitaxial growth but it does not attain the epitaxial growth temperature so the force of growth is offset by the force of growth of the densest C plane, thereby leading to a polycrystalline structure.

19

We then studied the substrate temperature dependence by evaluating the crystallization characteristics from the full-width at half the maximum of the (002) plane of hexagonal AlN obtained by X-ray diffraction measurement. Figure 4 shows the substrate temperature dependence of the full-width at half the maximum of the (002) plane. In this graph, o marks indicate the case of an Si(110) substrate, and □ marks indicate the case of a sapphire substrate. The crystallization characteristics of the Si(110) substrate increased following the temperature increase up to 600°C, but deteriorated above this temperature. This seems to be due to the reevaporization of aluminum. On the other hand, with the sapphire C-plane substrate, no special temperature dependence was observed up to 600°C, but improved crystallization characteristics were observed at 700°C, showing that this field still requires study.

We then studied the influence of the nitrogen ion beam energy by fixing the substrate temperature at 600°C. Figure 5 shows the relationship between the film deposition rate and the nitrogen ion beam energy. In this figure, the o marks indicate the case in which nitrogen ion beam is not assisted, that is, the case of Al film. As the nitrogen ion beam energy is increased, the film deposition rate decreases due to inverse-sputtering, and AlN film could not be obtained when the beam was assisted at above 1,000 eV. Figures 6 and 7 show the X-ray diffraction patterns of AlN films deposited on Si(110) and sapphire C-plane substrates. It was confirmed that the

Figure 4. Relationship Between Full-Width at Half Maximum of AlN (002) Plane and Substrate Temperature in XRD Analyses (o − Si(110) substrate, □ − sapphire C-plane substrate)

Figure 5. Relationship Between AlN Thin Film Deposition Rate and Nitrogen Ion Beam Energy (o − unassisted ion beam)

c-axis orientation was strongest at 200 eV with Si(100) and at 150 eV with the sapphire R plane, and that increasing the nitrogen ion beam energy degraded the crystallization characteristics but caused (110) orientation with the Si(110) substrate. The reason why the sapphire C plane is oriented at a lower energy than Si(100) may be because of the smaller number of mismatches and the low temperature dependence of crystallization characteristics.

Figure 8 [not reproduced] shows scanning electron microscope (SEM) photomicrographs of AlN films deposited on Si(110) substrates with various nitrogen ion beam energies. The AlN film surface contains noticeable unevenness with an energy of 100 eV, but it becomes sufficiently uniform at 150 and 200 eV so that electrode fabrication with submicrometer order is possible. When the energy is further increased to 250 or 300 eV, irregularities in crystalline structure and degradations of c-axis orientation are observed.
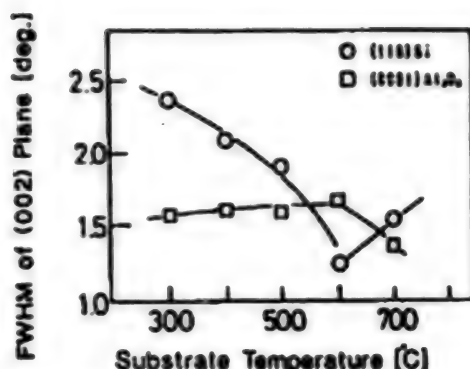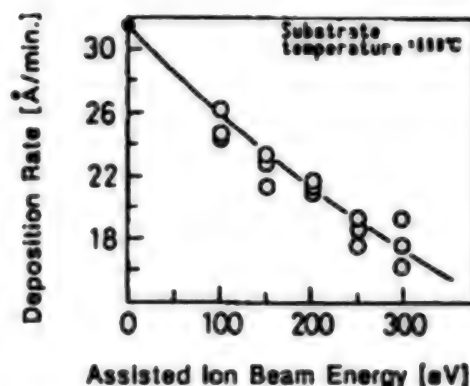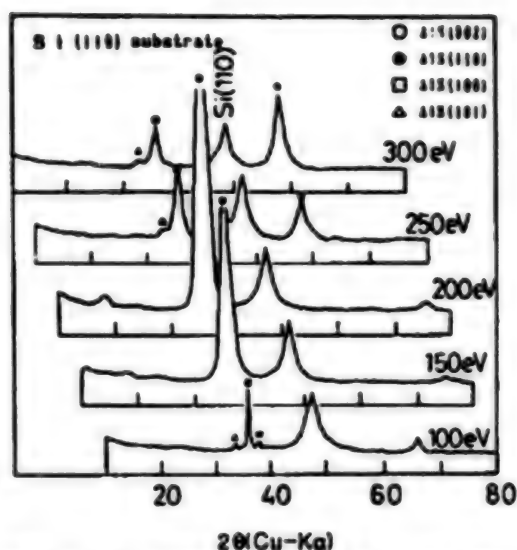
20

Figure 6. XRD Pattern of AlN Film
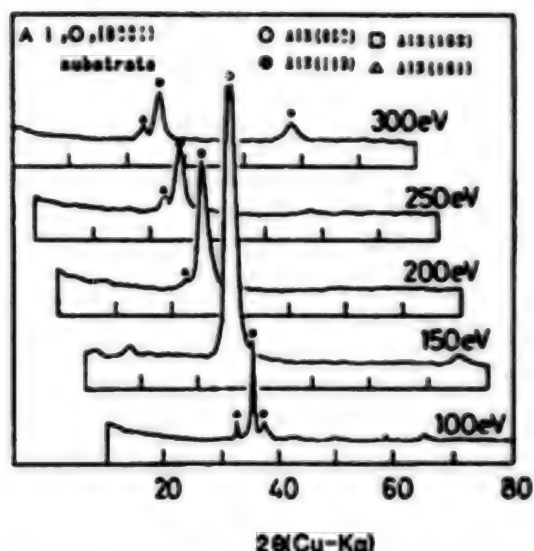(Substrate temperature 600°C,
Si(110) substrate)

Figure 7. XRD Pattern of AlN Film
(Substrate temperature 600°C,
sapphire C-plane substrate)

4. Applications in SAW Devices

The excellent electrical and mechanical properties of AlN thin films make them applicable in various fields.[8,9] The following description deals with their applications in SAW devices.

4.1 Surface Wave Characteristics

When applying thin films in SAW devices, we must consider that the characteristics of the surface waves vary greatly depending on the substrate type, crystal planes, propagation directions, electrode layouts, film thicknesses, etc., even when the films are of the same quality. Therefore, it is extremely important to predict the surface wave characteristics by means of simulation and other methods before producing prototype SAW devices. The simulation of surface wave characteristics of multilayer thin film structures are calculated using the equations of motion and electrostatic and piezoelectric basic formulas.[10] For details of the calculation methods, refer to reference 10. Here, we introduce the simulation results of the surface wave characteristics of single crystal AlN films deposited

Figure 9. Relationship Between
c-Axis Orientation Angle and
Phase Velocity
(Results of simulation assuming
KH = 2.7)

on Si(110) substrates, focusing on the relationship between the c-axis orientation angle and the phase velocity or coupling coefficient.
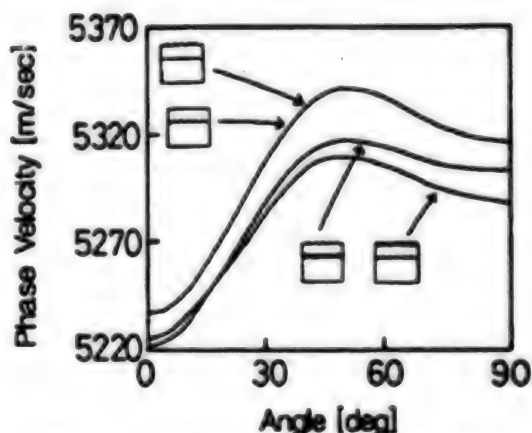
21

Figures 9 and 10 show the relationship between the c-axis angle (which is 0 degrees when the c-axis is perpendicular to the substrate) and the phase velocity and coupling coefficient, respectively, assuming that the KH (wave number x film thickness) parameter is equal to 2.7. The substrates were Si(110) and the propagation direction was (001), and the four electrode layouts shown in Figure 11 were used. With electrode (1), both the phase velocity and coupling coefficient were maximum with a c-axis angle of about 50 degrees. These results show that, in the application of AlN films in SAW devices, it is more advantageous that the c-axis is tilted by a certain angle than when it is grown perpendicularly to the substrate, or the (110) oriented film is more advantageous if we consider the coupling coefficient. In addition, as the film thickness and electrode pitch affect the phase velocity-versus-temperature characteristics and coupling coefficient greatly, designing each SAW device according to its final application is also important.
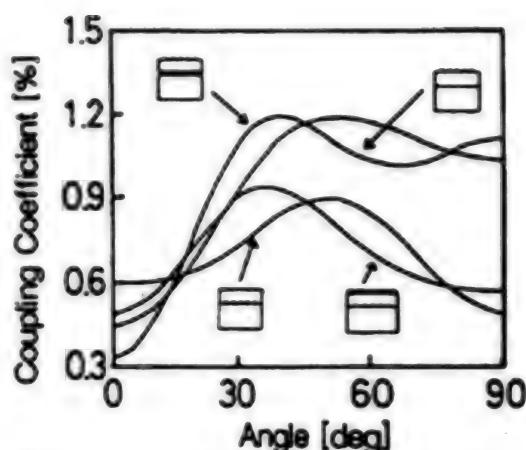

Figure 10. Relationship Between c-Axis Orientation Angle and Coupling Coefficient (Results of simulation assuming KH = 2.7)

In addition to improving the coupling coefficient by tilting the c-axis of AlN as described above, there are other reports on the use of a Sezawa wave which is a higher harmonic mode of a Rayleigh wave[11] and on the increase of coupling coefficient by forming a laminated structure with ZnO films featuring high coupling efficiency.[12]

Figure 11. Electrode Structures of Thin Film SAW Devices

On the other hand, it is also reported that a high phase velocity of 10,000 m/sec can be obtained with a laminated structure of AlN and diamond.[13]
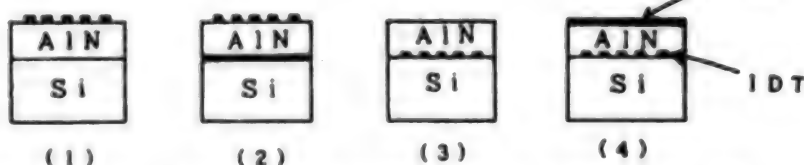
4.2 Result of SAW Device Prototyping

Figure 12 shows the characteristic of a SAW filter with IDT/AlN/Si(110) structure. The IDT has a multi-electrode structure with two pairs of input sections (63 x 2), a pair of output sections, an aperture length of

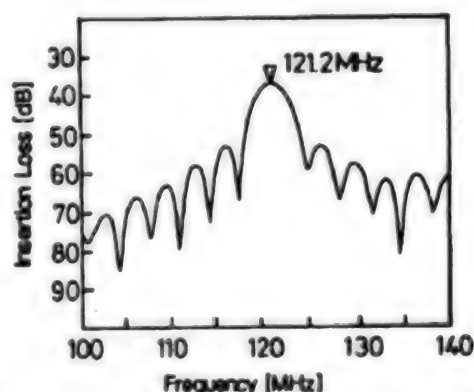Figure 12. Characteristic of SAW Filter With IDT/AlN/Si(110) Structure

22

1,160 μm and an electrode pitch ($\lambda/4$) of 9.3 μm. The phase velocity calculated from the center frequency (121 MHz) is about 4,500 m/sec, which is 10 percent lower than the simulated result. This seems to be because the mass load effect of the Al electrode for IDT was not taken into consideration in the simulation. The insertion loss is 38 dB and requires further reduction for practical use.

5. Conclusion

In the above, we introduced the fabrication of an AlN thin film by ECR dual ion beam sputtering and their application in SAW devices. Featuring a high-phase velocity that is not found in other materials, AlN thin films are promising materials for SAW devices for radio frequencies, but they also have a disadvantage which is their small coupling coefficient. For the implementation of SAW devices using AlN thin films in the future, electrode design will be as important as the establishment of the fabrication method of high-quality AlN thin film.

References

1. Kiyoshi Satoh, et al., JAPANESE JOURNAL OF APPLIED PHYSICS, Vol 29, Suppl. 29-1, 1989, p 157.

2. Mitsuyu, et al., DAI 25-KAI OYO BUTSURI GAKKAI KANKEI RENGO-KOENKAI YOK-SHU [Proceedings of the 25th Associated Seminar of the JSAP], 29a-A-4, 1978.

3. Shuskus, A.J., et al., APPL. PHYS. LETT., Vol 24, 1974, p 155.

4. Taylor, K.M., et al., J. ELECTROCHEM. SOC., Vol 107, 1960, p 308.

5. Shiosaki, T., et al., APPL. PHYS LETT., Vol 36, 1980, p 643.

6. Nickel, K.G., et al., J. AM. CERAM. SOC., Vol 72, 1989, p 1804.

7. Takagi, K., HYOMEN GIJUTSU [SURFACE TECHNOLOGY], Vol 41, 1991, p 22.

8. Manasevit, H.M., et al., J. ELECTROCM. SOC., Vol 118, 1971, p 1864.

9. Rutz, R.F., APPL. PHYS. LETT., Vol 28, 1976, p 379.

10. Campbell, J.J., IEEE TRANS. SONICS & ULTRASON., Vol 15, 1968, p 209.

11. Shiosaki, T., NIPPON CERAMICS KYOKAI GAKUJUTSU RONBUN-SHI [JOURNAL OF THE CERAMICS SOCIETY OF JAPAN], Vol 99, 1991, p 836.

12. Shiosaki, T., et al., IEEE ULTRASON. FERRO. & FREQ. CON., UFFC-33, 1986, p 324.

13. Yamanouchi K., et al., PROC. IEEE ULTRASON. SYMO, Vol 1, 1989, p 351.

Fabrication, Deposition of PZT and SrTiO₃ Film by Sputtering

[Article by Shuichi Komatsu and Kazuhide Abe, Research and Development Center, Toshiba Corp.]

[Text] 1. Introduction

As the integration of speed of LSIs are continuously improving, there is a strong demand to reduce the size of capacitors as well as the size of transistors and wiring. Needless to say, the use of dielectric materials with high dielectric constants is advantageous for reducing the size of capacitors Thin film capacitors using dielectric materials with high dielectric constants may be applied not only in DRAM memory cells, but also in a wide range of fields including chip capacitors and the bypass capacitors used in high-speed logic LSIs.

Research into ferroelectric materials of Pb(Zr,Ti)O₃ (PZT) has been active in recent years with a view to their applications in nonvolatile memories,[1] but SrTiO₃ which is a paraelectric material also has several advantageous properties that make it a promising material for use in thin film capacitors. This report is intended to introduce PZT and SrTiO₃ films as dielectric materials with high dielectric constants to be used in thin film capacitors, rather than in nonvolatile memories, and describes their fabrication methods and the results of experiments into their characteristics.

2. PZT Film

Silicon is one possible material for use as the substrate of thin film capacitors. However, because PZT tends to react easily with silicon, direct deposition on a silicon or silicon oxide substrate is difficult and a barrier layer should be installed. Pt is an effective material for this barrier layer, but it has a problem in adherence to the substrate. Therefore, this section deals with the results of a study on Pt-Ti alloy as the barrier layer material.

2.1 Comparison Between PZT Films on Pt and Pt/Ti Laminated Films

Before proceeding to the study of Pt-Ti alloy film, we first examined the barrier characteristic of Pt single-layer film (500 nm) and Pt (500 nm)/Ti (50 nm) laminated film. PZT films were deposited by simultaneous dual RF magnetron sputtering using $Pb(Zr_{0.70}Ti_{0.30})O_3$ and PbO sintered targets. The PZT deposition conditions were an RF power of 400 W with PZT and 200 W with PbO, a gas ratio between Ar/O_2 of 4/1 (flow ratio), a pressure of 1.1 Pa and a substrate temperature of 500°C. Pt and Ti were also deposited by RF magnetron sputtering. Figure 1 shows the X-ray diffraction pattern of the PZT films deposited on Pt and Pt/Ti. As shown in the figure, only the pyrochlore phase is produced on the Pt film while the Perovskite phase was also produced on the Pt-Ti film.
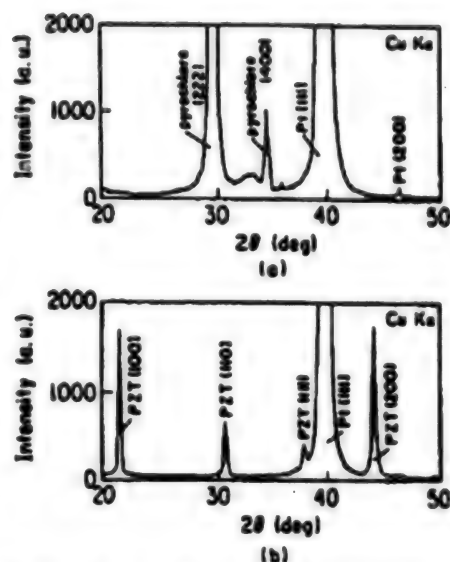

Figure 1. X-Ray Diffraction Patterns of PZT Thin Films
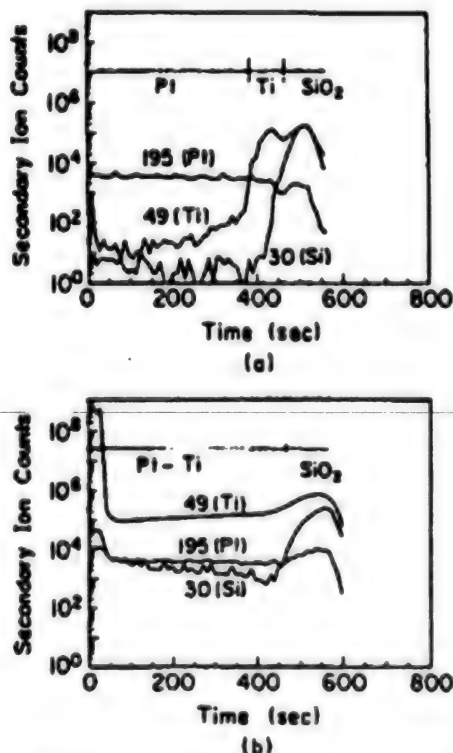(a) On Pt film
(b) On Pt/Ti film

Figure 2. SIMS Profiles in Depthwise Direction of Pt/Ti Thin Film
(a) Before thermal treatment
(b) After thermal treatment

To identify the cause of this, we formed Pt/Ti film on SiO_2, applied thermal treatment in Ar/O_2 at 500°C for 2 hours, and checked the behavior of Ti in the film. Figure 2 shows the scanning-type ion microscope (SIMS) profiles in the depthwise direction before and after the thermal treatment. The figure shows that a layer of Ti exists clearly between the Pt layer and SiO_2 before the thermal treatment. On the other hand, after the thermal treatment, Ti is diffused in the Pt and partially deposited on the surface. From this result, we presume that Ti diffused through Pt and reached the surface during PZT sputtering on the Pt/Ti film. Therefore, it unavoidably leads us to the conclusion that the Ti deposited on the surface plays a role in the formation of the Perovskite phase on the Pt/Ti film.

2.2 PZT Film on Pt-Ti Alloy Film

Then, we fabricated an alloy film of Pt and Ti for use as the barrier layer on heat-oxidized silicon by sputtering, and deposited a PZT film on it. The Pt/Ti alloy film was fabricated by simultaneous dual sputtering using Pt and Ti targets. The Pt target was supplied

with a constant power of 300 W, the Ti target was supplied with a variable power from 0–450 W, and we fabricated several alloy films with different Ti/Pt ratios by varying the power supplied to the Ti target. The sputtering gas was Ar, the pressure was 0.5 Pa, and the substrate was not heated. On Pt/Ti alloy films with different composition ratios fabricated with the above conditions, we deposited PZT film by sputtering with a uniform condition (which is the same as the condition described in section 2.1), and investigated the crystalline structure of the PZT films obtained by X-ray diffraction. Table 1 shows the relationship between the composition of Pt–Ti alloy films formed as the barrier layer and the crystalline structure of the PZT films deposited on them. The formation of the Perovskite phase is observed with Pt–Ti alloy film composition ratios between 0.02–0.17. The pyrochlore phase is formed when the ratio of Ti is smaller than this range, and lead oxide is formed when it is larger. The compositions of the Pt/Ti films and those of PZT films, mentioned later, are determined by inductively coupled plasma (ICP) emission spectro-scopy.

Table 1. Relationship Between Ti/Pt Ratio and PZT Crystalline Structure

Pt power (W)	Ti power (W)	Ti/Pt ratio (atm. ratio)		PZT crystalline structure
300	0	0		Pyrochlore
300	50	0	02	Perovskite
300	100	0	14	Perovskite
300	150	0	17	Perovskite
300	200	0	22	Perovskite + PbO
300	300	0	32	PbO
300	450	0	47	PbO

Figure 3 shows the variation of the so-called A/B ratio, that is, the ratio between Pn/(Zr+Ti), of PZT film depending on the composi-tion ratio of the Pt–Ti alloy film used as the barrier layer. In the Ti/Pt ratio range in which the PZT film has a Perovskite phase, the Pb/(Zr+Ti) ratio is almost constant (at 1.2). The Pb/(Zr+Ti) ratio is no more than 1 in the range in which the PZT film has a pyrochlore phase, and no less than 2.5 in the range in which the PZT film is lead oxide.

2.3 Considerations on Effects of Ti on Substrate Surface

As described above, if only Pt film is used as the barrier layer, the PZT film has only a pyrochlore phase, and PZT film with the Perovskite phase is obtained only in case a proper amount of Ti is contained on the Pt
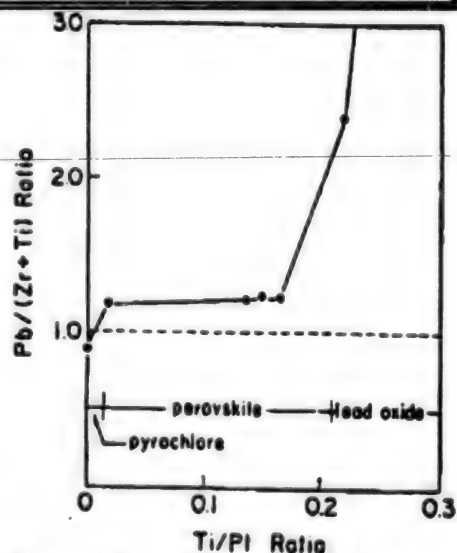

Figure 3. Relationship Between Barrier Layer Composition (Ti/Pt Ratio) and PZT Composition (Pb/(Zr+Ti) Ratio)
(PZT: 400 W; PbO: 200 W)

film. Now, we will consider how the presence of Ti in Pt film is involved in the generation of the Perovskite phase. As shown in Figure 3, in the case when a pyrochlore layer is generated, the composition of the deposited film lacks Pb. However, in the Ti/Pt ratio range in which the PZT film has a Perovskite phase, the Pb/(Zr+Ti) ratio in PZT film is larger than 1, at 1.2. From the stoichiometric viewpoint, this fact indicates that the Perovskite phase can be generated only when the quantity of Pb entering the A site is excessive. This leads us to think that the presence of Ti in Pt film has the effect of restricting the re-evaporation of Pb atoms from the substrate during nucleation in the initial stage of film formation, and that this contributes to the generation of the Perovskite phase.

We then investigated whether a Perovskite phase is generated or not if the supply of Pb is decreased during the deposition of the PZT film on a barrier layer with a constant Pt/Ti ratio (about 0.1). The Pb supply was regulated by varying the power supplied to the PbO target during sputtering, without varying the power supplied to the PZT target. The crystalline structure of the PZT film obtained showed that a pyrochlore layer is generated when the Pb supply is low as shown in Table 2.

Table 2. Relationship Between PbO Power and PZT Crystalline Structure

PZT power (W)	PbO power (W)	PZT crystalline structure
400	50	Pyrochlore
400	100	Pyrochlore + Perovskite
400	150	Perovskite + Pyrochlore
400	200	Perovskite

This means that, to obtain PZT film with a Perovskite phase, Pb should be excessive to a certain degree even when Ti is present on the substrate surface. The experiment in which the supply of Pb was varied on the Pt film did not generate a Perovskite phase. This result made it clear that, to obtain PZT film with a Perovskite phase, Ti should be present on the substrate surface and Pb should be excessive.

3. SrTiO$_3$ Film

Compared to PZT, as a capacitor material, SrTiO$_3$ features the following advantages: 1) smaller variation with time of dielectric constant because it is not ferroelectric (has no domains) at room temperature; 2) better frequency characteristics; and 3) more chemically stable. There is old research on SrTiO$_3$ thin film by Pennebaker,[2] but many new announcements have been made in recent years taking notice of the advantages listed above.[3] The description in the following covers the results of our investigations into the basic properties, such as the crystallization temperature and the relationship between the crystallinity and dielectric characteristic of the film, of SrTiO$_3$ films fabricated by sputtering.

27

3.1 Methods of Film Fabrication and Evaluation

We fabricated $SrTiO_3$ film by RF magnetron sputtering, using a $SrTiO_3$ sintered substance as the target and silicon as the substrate material. The sputtering conditions were an RF power of 400 W, a gas ratio between $Ar_{/O}2$ of 4/1 (flow ratio), a pressure of 1.2 Pa, substrate temperatures

Figure 4. Structure of Electrical Property Measuring Capacitor

from room temperature to 600°C, and a sputtering time of six hours. We then evaluated the fabricated $SrTiO_3$ in terms of the crystalline structure, composition, microstructure and electrical properties. The crystalline structure was tested by X-ray diffraction, the composition by ICP emission spectroscopy, and the microstructure, with a transmission electron microscope (TEM). As for the electrical properties, the bias voltage dependence of electrostatic capacity (C-V characteristic) and the voltage dependence of leakage current (I-V characteristic) were evaluated at room temperature. For the electrical property evaluation, we made a thin film capacitor by fabricating an Au/Cr upper electrode by evaporation and lift-off. The structure of the thin film capacitor used in the electrical property measurements is shown in Figure 4.
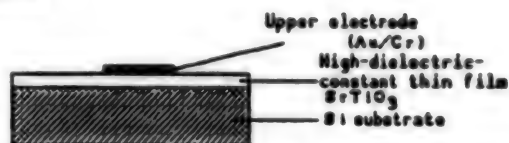
3.2 Crystalline Structure and Composition of $SrTiO_3$ Film

Figure 5 shows the X-ray diffraction patterns of $SrTiO_3$ films deposited with substrate temperatures from 200□600°C. The figure shows that $SrTiO_3$ with a Perovskite phase is generated with substrate temperatures of 300°C or more. As the substrate temperature rises, the peak intensity increases, indicating the progress of the degree of crystallization. with regard to the film orientation observed with the film deposited at 600°C, peaks are present in (200) and (111) in addition to the maximum peak at (110), showing that there is no orientation in a specific direction. Figure 6 shows the substrate temperature dependence of the Sr/Ti composition ratio of the $SrTiO_3$ film deposited. As shown in the figure, with substrate temperatures from room temperature

Figure 5. X-Ray Diffraction Patterns of $SrTiO_3$ Films Deposited While Varying Substrate Temperature

to 600°C, the Sr/Ti ratio does not vary regardless of the substrate temperature and is close to the target composition (Sr/Ti - 1.0). This may be because the re-evaporation of Sr and Ti from the substrate are small with substrate temperatures up to 600°C, which indicates that the composition control of $SrTiO_3$ film by sputtering is easier than the control of PZT film described above.

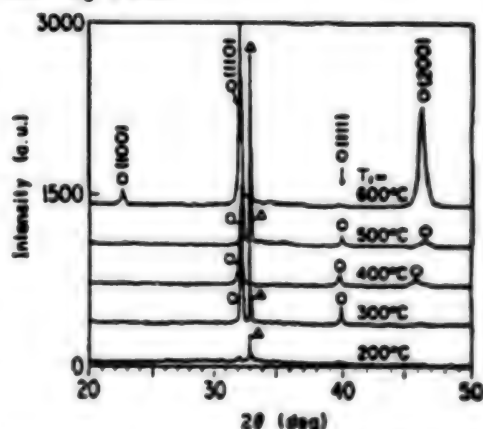As for the electrical properties of $SrTiO_3$ thin film with a Perovskite phase, it is possibly sensitive to the so-called A/B ratio (Sr/Ti ratio) so the ease of composition control can be regarded as one of the advantages in the deposition of $SrTiO_3$ by sputtering.
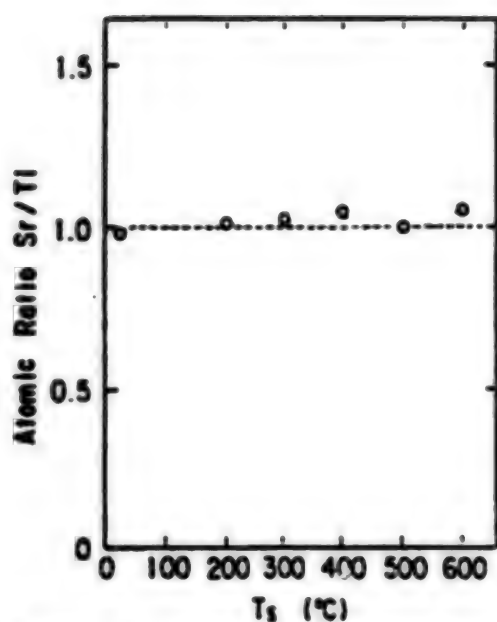
28

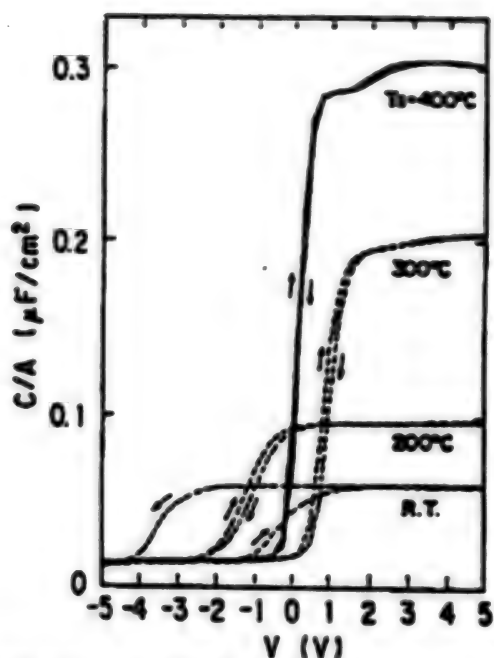Figure 6. Substrate Temperature Dependence of Sr/Ti Composition Ratio

Figure 7. Substrate Temperature Dependence of C-V Characteristic of SrTiO$_3$ Film

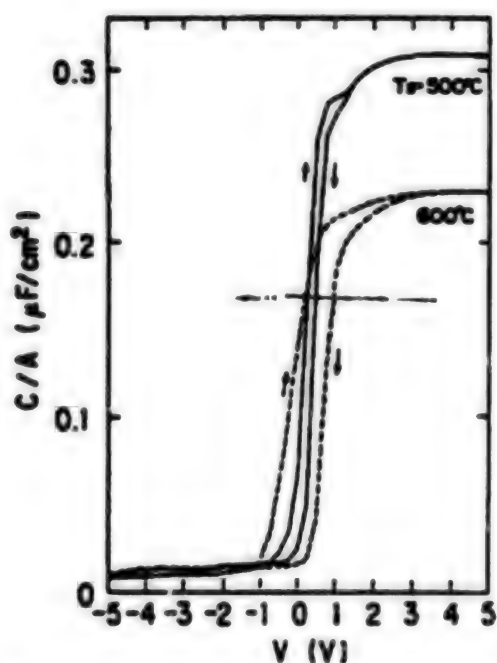Figure 8. Substrate Temperature Dependence of C-V Characteristic of SrTiO$_3$ Film

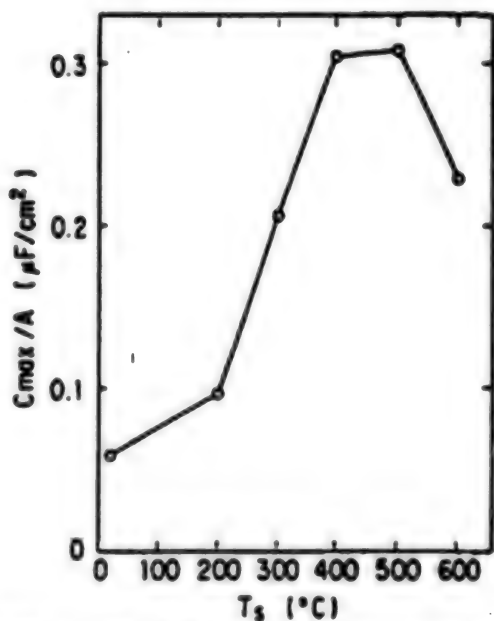Figure 9. Substrate Temperature Dependence of C$_{max}$ of SrTiO$_3$ Film

29

3.3 Electrical Properties

(1) C-V characteristic

Figures 7 and 8 show the bias voltage dependence of electrostatic capacity measured at 1 MHz (C-V characteristic) of $SrTiO_3$ films fabricated on n-type silicon substrates, and Figure 9 shows the relationship between the maximum electrostatic capacity (C_{max}) measured above and the substrate temperature during deposition. The value of C_{max} increases with the increase of substrate temperature from room temperature-500°C and, when this data is compared to the results of X-ray diffraction, there seems to be a certain relationship with the degree of crystallization. This can also be predicted qualitatively from the fact that the largest part of the high dielectric constant of $SrTiO_3$ derives from ionic polarization. We investigated the reason why the capacity of the film deposited at 600°C is small in spite of the good degree of crystallization using a TEM, and found that it was due to the formation of SiO_2 at the interface between the silicon substrate and $SrTiO_3$.

With the C-V characteristics shown in Figures 7 and 8, there is no capacitance when a negative bias voltage is applied. This is because the n-type silicon used as the lower electrode produces a depletion layer near the silicon substrate surface and the depletion layer has a parasitic capacitance in series with the $SrTiO_3$ film. The hysteresis observed in the C-V characteristic indicates a drift of ions inside the film or the presence of charge traps in the film. From the direction in which the hysteresis curve is curved, the cause of the hysteresis is thought to be the ion drift in the low substrate temperature range, and charge injection in the high substrate temperature range.

(2) Leakage current characteristic

Figure 10 shows the substrate temperature dependence of the leakage current when voltages of 5 and 3 volts are applied so that the upper electrode is positive. The leakage current of the film fabricated at room temperature is large, and the cause of this is thought to be the higher ratio of ion current due to the amorphous structure of the film. Let us consider the substrate temperature dependence of the leakage current shown in Figure 10 considering the equivalent circuit shown in Figure 11, by also taking the results of TEM observations described above into consideration.

Assuming that the current flowing through the $SrTiO_3$ film is the sum of the ion current (I_{ion}) and electron current ($I_{electron}$), these currents are represented by parallel resistors in the equivalent circuit, and the resistance
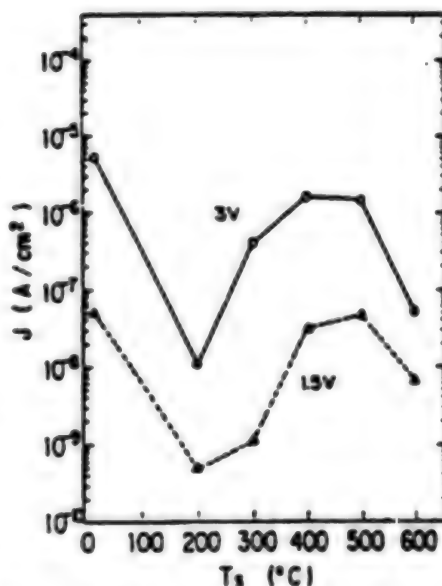

Figure 10. Leakage Current Characteristic of $SrTiO_3$ Film

30

derived from the SiO_2 layer at the interface (R_{SiO_2}) can be regarded as being connected in series to these resistors. As shown in Figure 12, $SrTiO_3$ films fabricated at substrate temperatures under 500°C do not have an SiO_2 layer at the interface, so R_{SiO_2} is small enough to be ignored. In this range, a higher substrate temperature during film fabrication can improve the crystallization characteristics and decrease the ion current, but high substrate temperatures also increase oxygen defects and the electron current. In this way, the ion current is dominant at the lower temperature range (Range I) while the electron current is dominant at the higher temperature range (Range II). On the other hand, in the substrate temperature range above 500°C (Range III), the SiO_2 layer formed at the interface functions as a barrier, so the capacity deceases but the leakage current also decreases.

4. Conclusion

We described the influence of the barrier layer in the fabrication of PZT film by sputtering and the structure and characteristics of $SrTiO_3$ film fabricated by sputtering. Which of these materials are more suitable for use in thin film capacitors should be determined based on the results of future research, but we believe that the key points in the development of materials to deal with element size reduction and speed increase lie in the reduction of leakage current and the improvement of the frequency characteristics of the dielectric constant. Research focused on these points is desirable in the future.

Figure 11. Equivalent Circuit of Leakage Current
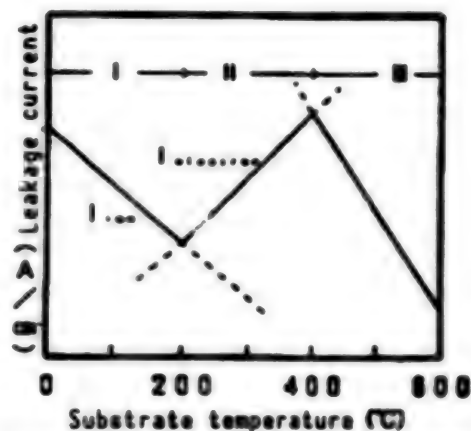
Figure 12. Substrate Temperature Dependence of Leakage Current
  I Range in which ion current is dominant
  II Range in which electron current is dominant
  III Range in which interface resistance is dominant

References

1.   Scott, J.F., et al., SCIENCE, Vol 246, 1989, p 1400.

2.   Pennebaker, W.B., IBM J. RES. DEVELOP., Vol 13, November 1989, p 686.

3.   For example, S. Matsubara, et al., MAT. RES. SYMP., Vol 200, 1990, p 243.
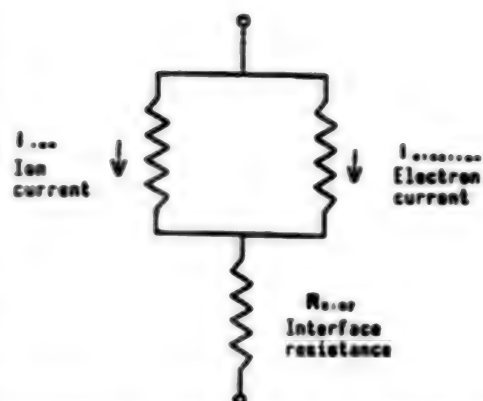
PZT Film Properties, Application to Memory by Sputtering Method

[Article by Kazunori Torii, Toru Kaga, Keiko Kushida, and Eiji Takeda, Hitachi Central Research Laboratory]

[Text] Recent progress in film formation technology has made the application of ferroelectric substances in memory more realistic than ever, and active R&D is being conducted by research organs inside and outside Japan. Applications of ferroelectric substances in memories mainly consist of nonvolatile memories utilizing the polarization reversal and of DRAM capacitor insulation films utilizing the high dielectric constants. This report first describes the topics concerning the application of ferroelectric thin films in DRAMs then introduces the results of experiments conducted by the authors.

1. Cell Structure and Technical Topics Concerning Ferroelectric DRAMs

(1) Changes of Quantity of Charge Stored in DRAM Cells

Figure 1 shows the changes of stored charge quantity, Q, of recent DRAM cells. DRAMs below the 1-megabit class could maintain the stored charge quantity Q by compensating for the decrease of capacitor surface area (about one-third per generation) with the reduction of capacitor insulation film thickness (about one-third per generation). However, because the reduction of capacitor insulation film thickness started to approach the limit above 1-megabit DRAMs and that the internal operating voltage started to drop above 16-megabit RAMs, the stored charge quantity tends to decrease by about 30 percent per generation, in spite of introduction of various three-dimensional structures.
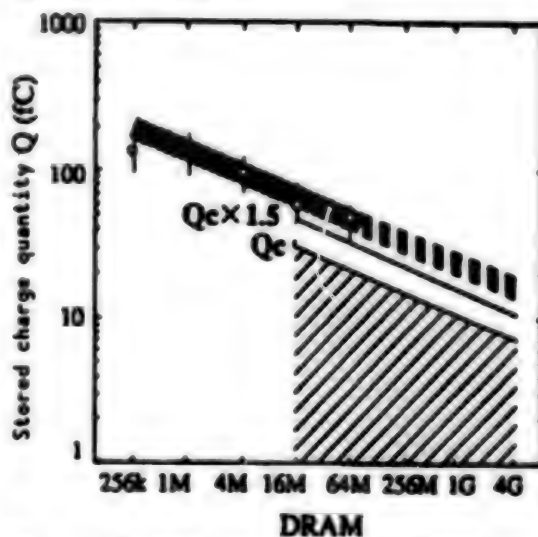

Figure 1. Changes in Stored Charge Quantities of DRAM Cells (Based on data published by ISSCC and IEDM)

DRAM cells which store data as charges should store sufficient charge to deal with:

1) leakage of stored charge due to leakage current;

2) sense amplifier malfunctions due to circuit noise;

3) destruction of capacitor stored charge due to the penetration of noise charges derived from α rays (soft errors); and so on.

Among these phenomena, the leakage current may be reduced by decreasing the power and improving the film quality, and sense amplifier malfunctions may be improved by suitable circuit design, but soft errors which are dependent on natural radiation are the last obstacle to the normal operation of memory cells. The design of memory cells is therefore required to maintain the resistance to soft errors. The critical charge quantity required to prevent soft errors, QC, should be around 30 fC in a 16-megabit DRAM, for example.[1] If the charge quantity stored in a memory cell is to be designed so that it has a margin of about 50 percent with respect to the critical charge quantity taking the variations in the capacitor surface area and insulation film thickness due to supply voltage variations and fabrication variations into consideration, the charge quantity should be at least 45 fC in a 16-megabit DRAM. This value almost coincides with the minimum storage capacity value of memory cells announced by manufacturers for use in 16-megabit DRAMs, so it can be regarded as an optimum value of the minimum target of stored charge. As the critical charge is almost proportional to the width of the depletion layer,[2] it is believed to decrease in proportion to the memory cell size, or to 0.6-0.7 fold per generation. As a result, the change of stored charge as we approach gigabit generations in the future should also aim at changes of the critical charge quantity (which is about 0.7 fold per generation).

(2) Memory Cell Structure

Ferroelectric materials are expected to cut the development and manufacturing costs of DRAM memory cells by making their structures, which are getting more and more complicated, simple again. The simplest DRAM memory cell structure is the planar structure, but this structure requires the fabrication of the capacitor before the switch element. In this case, to form the channel section of the switch element, a ferroelectric thin film should be deposited on the substrate surface first, then it should be removed by etch-

Figure 2. Data Line Shielded Flattened STC Cell

ing before formation. Such a process presents problems including the etching damage of the channel section, contamination of the substrate, and the influence of high temperatures during gate oxidation of the ferroelectric thin film and barrier metal.
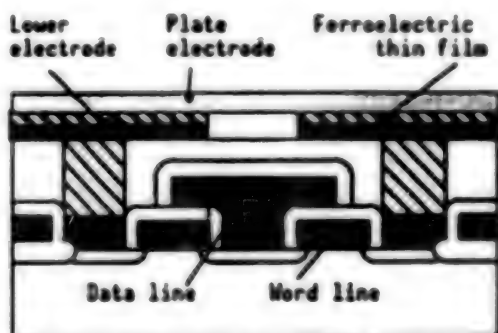
A memory cell structure which is suitable for use with ferroelectric thin film thanks to the larger capacitor area and relatively simpler structure than the planar structure is the flattened STC cell of the data line shielded type shown in Figure 2.

This structure has the following advantages:

1) a capacitor area about half the cell area can be assured;

2) the possibility of damage or contamination during deposition is low because the ferroelectric thin film is isolated from the switch element below it;

3) film deposition is easy because the capacitor insulation film and storage node are formed on a flat surface;

4) data line noise can be reduced to about a quarter; etc.[3]

Figure 3 shows the relationship between the relative dielectric constant and film thickness which are required to implement 16-megabit and higher DRAMs using this memory cell structure. If a relative dielectric constant similar to bulk ceramics can be maintained even when the film thickness is decreased to about 10 nm, it may be possible to implement 1-4 gigabit DRAMs using $SrTiO_3$, $(Ba,Sr)TiO_3$ or up to 16-gigabit DRAM using PZT.

Figure 3. Relative Dielectric Constant and Film Thickness of Capacitor Insulation Films Required for DRAMs of Several Generations When Flattened STC Cells Are Used

(3) Limit of Reduction of Ferroelectric Film Thickness

The relationship between the relative dielectric constant and film thickness which are required to implement DRAMs of different generations is shown in Figure 3. Which generation each ferroelectric material can be used in is determined by how far the thickness of the film of each ferroelectric material can be reduced.

One of the factors determining the limit of film thickness reduction is the limit of insulation. Figure 4 shows the strength of the maximum electric field (withstand voltage) E_{max} which can be applied to various insulation films as a function of their relative dielectric constants E. With paraelectric materials, E_{max} usually decreases in proportion to the square root of E.[4] Therefore, to maintain sufficient insulation, films with higher dielectric constants should have greater thicknesses provided that the electric field is constant. Data for ferroelectric thin films is not sufficient, but their characteristics show the same trend according to the results reported up to now.[5]
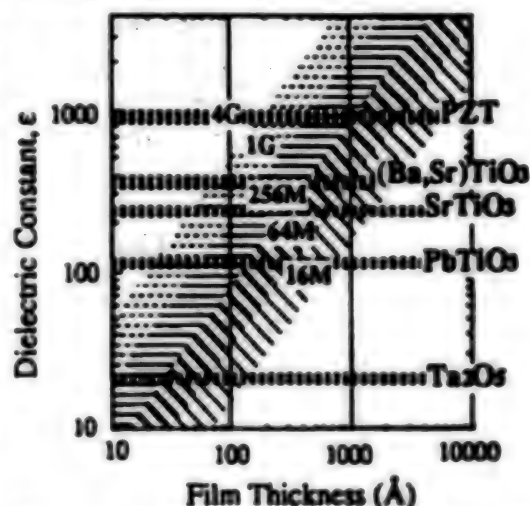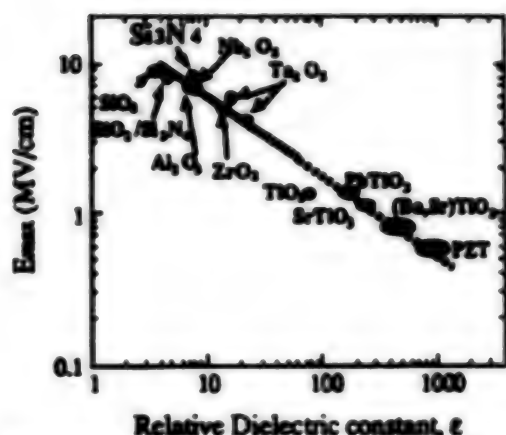
Figure 4. Relationship Between Withstand Voltage and Relative Dielectric Constant of Various Insulation Films

Figure 5. Relationship of Film Thickness Required in Different DRAM Generations, Film Thickness Reduction Limits for Different Withstand Voltages, and Film Thickness Ranges Usable With Three-Dimensional Cells

Figure 5 shows the relationship between the ferroelectric thin film thickness required for a flattened STC cell and the film thickness reduction limit imposed by the withstand voltage based on Figure 4. The graph shows that the film thickness reduction limit imposed by the withstand voltage decreases slightly following the scaling of the supply voltage.

The solid lines in the graph indicate the film thicknesses required when fabricating flattened STC cells using materials with different relative dielectric constants. This data means that dielectric constants of respective generations can be implemented if it is possible to fabricate a thin film with the corresponding dielectric constant and a thinner film thickness than the film thickness indicated by the solid line. The dotted lines in the graph indicate the limit of film thickness reduction imposed by the withstand voltage. By using flattened STC cells, memory cells capable of storing the charge necessary for circuit operation can be implemented until the position where the dotted line crosses the solid line.

For example, the use of thin film with a dielectric constant of 1,000 offers the possibility of implementing 16-gigabit DRAMs using flattened STC cells.

(4) Three-Dimensional Cells Using Ferroelectric Thin Film

The first technical topic to be considered in the use of ferroelectric thin film in three-dimensional cells may be the technology for formation of the lower electrode. Many materials are being studied for use as the lower electrode, but it is reported that direct formation of ferroelectric thin film on polycrystalline silicon is difficult and that a metal barrier made of Pt, Pd or their Ti alloy is required.[6] As a result, in case three-dimensional cells are to be used, both the metal barrier and ferroelectric material should be formed on the side walls of three-dimensional capacitors.
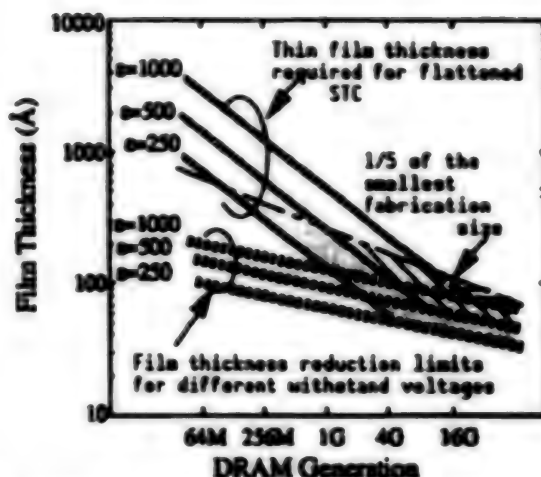
35

The film deposition method used may be chemical vapor deposition (CVD) with its excellent irregularity coating characteristic, but this requires the development of CVD technology for barrier metals as well as for ferroelectric materials.

The thicknesses of ferroelectric thin film and barrier metal also pose problems in implementing three-dimensional capacitors. Let us assume that the barrier metal can be made thin so it is the same thickness as the ferroelectric thin film. As the capacitor interval is designed with minimum fabrication size, film thickness t of the ferroelectric film and barrier metal should be less than one-fifth of minimum fabrication size f. Otherwise, if it is thicker than this, the interval with the adjacent capacitor would be filled, making it impossible to form the plate electrode. The alternate long and short dash line in Figure 5 indicates f/5. Since the solid lines in the figure indicate the maximum film thickness for fabricating flattened STC cells, the use of three-dimensional cells is not necessary if a thinner film than it can be fabricated. But the film cannot be thinner than the film thickness reduction limit which is indicated by dotted lines As a result, the use of three-dimensional cells emerges in case it is only possible to fabricate films with the thickness in the hatched section, that is, located above the solid and dotted lines and below the alternate long and short dash line. For example, when ferroelectric thin film with E - 1,000 is used, the use of three-dimensional cells is possible from 16-gigabit DRAM and later. With a material with E - 250, the film thickness range which requires the use of three-dimensional cells is larger. Since it is not easy to introduce new materials at every generation, the development of a ferroelectric DRAM should be started after deciding whether flattened STC cells are to be used by using materials with a high dielectric constant from the beginning or a material with which thin film deposition is easy even if its dielectric constant is not so high is to be selected first and the design is to be switched to three-dimensional cells later.

2. Deposition of PZT Thin Film by Single-Target Sputtering

As a material which can implement 1-16 gigabit DRAMs in the form of flattened STC cells with a simple process, we selected PZT and are conducting experiments into film deposition by RF sputtering. The following describes the results of recent experiments.

(1) Thin Film Deposition

We used PZT sintered substances as the target. The Zr/Ti composition ratio is 49.7:50.3, and PbO is contained excessively by 15 mol percent.

For the substrate, thermal oxidized film of about 1,000 Å is formed on a p-type silicon substrate then a platinum film of 1,000 Å is formed on it by DC sputtering. The sputtering condition of the PZT thin film is shown in Table 1.

Table 1. PZT Thin Film Sputtering Condition

Sputtering gas	Ar/O_2 (0/10)
Sputtering gas pressure	15 (Pa)
Rf -power	200 W
Substrate temperature	200°C
Target	$Pb(Zr_{50}Ti_{50})O_3$ + PbO 15 mol%
Target size	4 inches
Target-Substrate distance	30 mm

(2) Thin Film Composition Control

Figure 6 shows the sputtering gas pressure dependence of the ratio of metallic elements. The thin film composition was measured by inductively coupled plasma spectroscopy (ICPS).

On the low sputtering gas pressure side, the ratio of lead is lower than the lead ratio of the target, and it increases together with the gas pressure to approach the value of the target. We consider that the cause of such a change in the lead content is its selective resputtering by high-speed negative ions which are accelerated by electric field and strike the substrate. On the other hand, the ratios of zirconium and titanium are constant regardless of the sputtering gas pressure.

Our experiments proved that the thin film with almost the desired composition can be obtained with a gas pressure of around 15 Pa. With gas pressure around 15 Pa, the average free path of particles is in the millimeter order and the occurrence of high-energy negative ions decreases. As a result, the selective resputtering of lead is reduced and the composition variation becomes small. We also believe that there is another advantage which is the restriction of thin film damage due to the collision of high-energy ions.

Figure 7 shows the change of the ratio of metallic elements in the film depending on the RF power. The figure shows that increasing
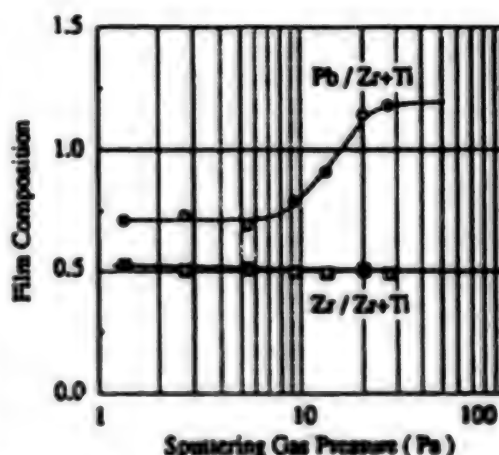

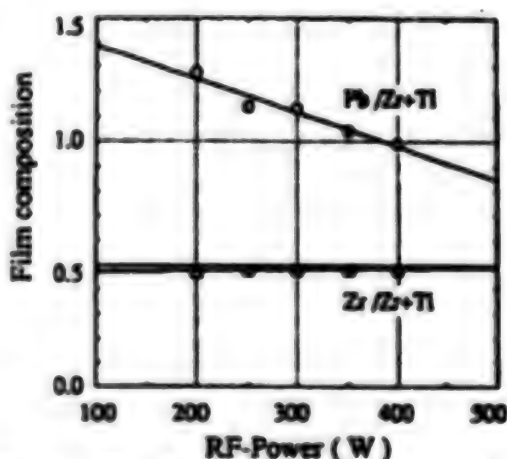Figure 6. Sputtering Gas Pressure Dependence of PZT Thin Film Composition

Figure 7. RF Power Dependence of PZT Film Composition

37

the RF power decreases the lead composition proportionally. We believe that the decrease of lead content is due to a similar cause to the above, that is, lead resputtering from the substrate by high-energy particles.

Because only the ratio of lead can be changed proportionally to the RF power while the ratios of zirconium and titanium barely change and that the RF power can be controlled more easily and accurately compared to the sputtering gas pressure, the content of lead in thin film can be subjected to strict control by the RF power.

(3) Crystalline Structure Change Due to Thermal Treatment

The relative dielectric constant of the as-depo film is about 175, and it is believed that PZT is contained in the film. However, as the film has a large leakage current and low withstand voltage as it is, it should be processed by thermal treatment in an oxidizing atmosphere so that it can become a film with sufficient insulation.

We conducted a high-temperature X-ray diffraction experiment to identify the change of the crystalline structure of PZT thin film during thermal treatment (Figure 8).

The first crystalline structure change occurs at 480°C. The peak observed on the as-depo film starts to disappear, and a new peak appears with a scattering angle of 33.5 degrees. This crystalline structure change takes place slowly. When a temperature of 480°C is maintained, only the peak at 33.5 degrees is observed about three hours later. At temperatures from 480-580°C, we could observe that the intensity of the 33.5-degree peak increased gradually and its width narrowed.
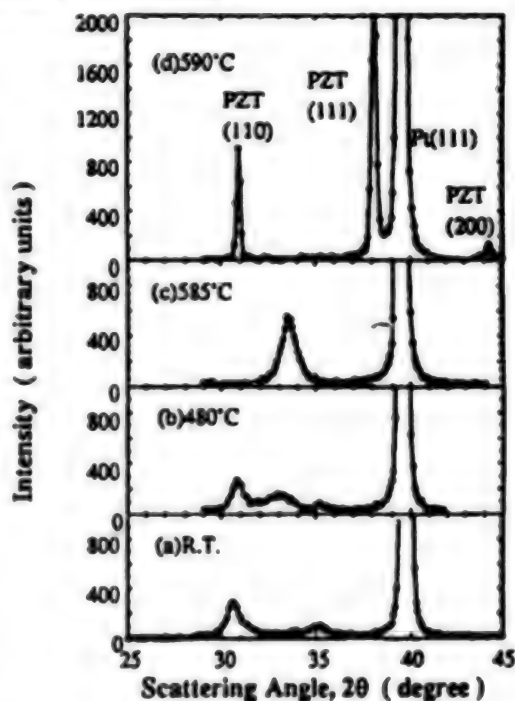

Figure 8. PZT Thin Film Crystalline Structure Changes by Thermal Treatment
(Changes in X-ray diffraction graphs of high-temperature X-ray diffraction)

At 590°C, the 33.5-degree peak disappeared and the peak of a rhombohedral Perovskite structure appeared. This second crystalline structure change occurs very quickly compared to the first crystalline structure change. A sharp peak appears from the beginning, and the intensities and widths of the peaks hardly change later. Based on these results, we decided to apply thermal treatment at 600°C for two hours.

38

(4) Electrical Properties

Figure 9 shows the film composition dependence of the relative dielectric constant and resistivity (with 5 volts applied) of PZT thin film. The figure shows that a change of lead content by only 1.2 percent causes large changes in the relative dielectric constant and resistivity of PZT thin film.
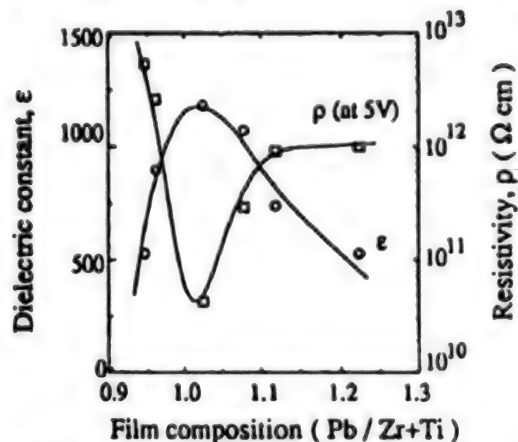

Figure 9. Composition Dependence of Relative Dielectric Constant ϵ and Resistivity ρ of PZT Thin Film
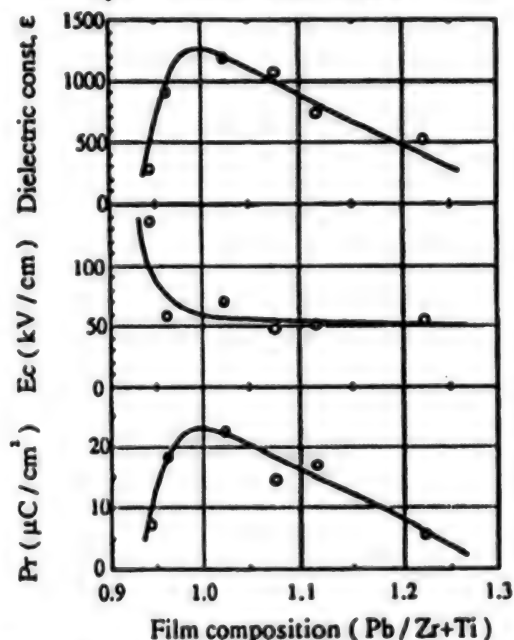

Figure 11. Film Thickness Dependence of Relative Dielectric Constant and Crystalline Orientation of PZT Thin Film

Figure 10. Composition Dependence of Relative Dielectric Constant ϵ, Coercive Electric Field E_c, and Remanent Polarization P_r of PZT Thin Film
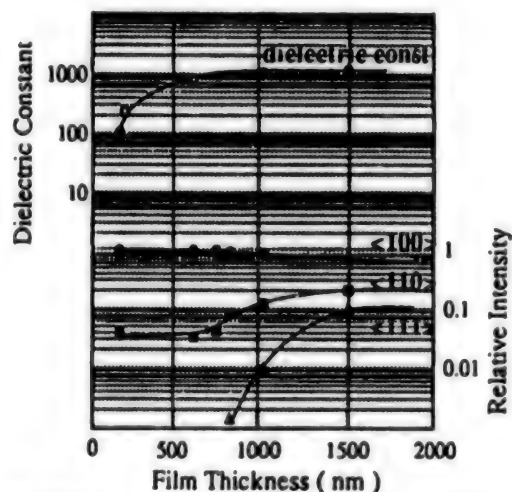
Figure 10 shows the film composition dependence of the relative dielectric constant, remanent polarization and coercive electric field. The figure shows that there is a good correlation between the dielectric constant and remanent polarization, with both of them attaining the maximum values when $Pb/(Zr+Ti) = 1$. The relative dielectric constant of a film with $Pb/(Zr+Ti) = 1$ is about 1,180, the coercive electric field is 52 kV/cm, the remanent polarization is 22.5 $\mu C/cm^2$, all of which are similar values to bulk PZT.

Figure 11 shows the film thickness dependence of the relative dielectric constant and crystalline orientation intensity. The relative dielectric constant is constant at film thicknesses of 1 μm or more but, when thinner, it decreases together with the film thickness.

The decrease of film thickness also affects the crystalline orientation. With thicker films, it is close to the X-ray diffraction pattern of a random-oriented polycrystal and peaks at (100), (110), (111), and (200) are observed. However, as the film thickness decreases, the diffraction intensities of peaks (100) and (200) increase. When the film thickness is below 200 nm, only peaks (100) and (200) are observed and the film becomes a (100) orientation film. We believe that the crystalline orientation change accompanying the decrease in film thickness is also a cause of the decrease of dielectric constant.

References

1. Kimura, S., et al., IEEE TRANS. ON ELECTRON DEV., 1988, pp 596–599.

2. Hu, C., IEEE ELECTRON DEV. LETT., 1982, pp 31–34.

3. Aoki, M., et al., ISSCC DIG. TECH. PAPERS, February 1989, pp 238–239.

4. Sunami and Asai, HANDOTAI KENKYU, Vol 24, Kogyo Chosakai [Semiconductor Research Industrial Institute], 1986, pp 51–84

5. Schuele, P.J. and Traynor, S.D., Abstracts of the 5th U.S.–Japan Seminar on Dielectric and Piezoelectric Ceramics, 1990, pp 286–289.

6. Sakuma, T., et al., APPL. PHYS. LETT., Vol 57, 1990, pp 2431–2433.

PZT Thin Film Fabrication by MOCVD, Application in Memory Devices

[Article by Hiromi Ito, Keiichiro Kashiwabara, Tomohito Okudaira, Takashi Higaki, and Katsuhiro Tsukamoto, LSI Laboratory, Mitsubishi Electric Co., Ltd.]

[Text] 1. Introduction

In the production of DRAMs where the reduction of costs through economies of scale is the theme, to be "simple and easy to make" has an important significance. However, the reduction of the area which capacitors occupy due to higher levels of integration has forced the adoption of three—dimensional memory cell structures, resulting in increases in the number of processes as well as factors degrading yield. The introduction of tantalum oxide is being studied as a film material with a high dielectric constant that can replace silicon nitrides, but the use of three—dimensional structures is unavoidable with 64M DRAMs and later.

The application of PZT in nonvolatile memories based on ferroelectricity has been proposed for a number of years, and recent studies into its application in DRAMs can be regarded as being based on the general recognition of the technical bottleneck in current DRAM fabrication processes which have become too complicated. If the very large relative dielectric constant of PZT can be used in the storage of charge, it is expected that perfectly plain capacitors with a simple structure could be implemented even at the 256M level and that the life of current dielectric constant designs can be extended to 1—gigabit DRAMs and later. Ferroelectricity can be regarded as a factor bringing about a new added value to DRAMs in the future, but it is a subject of concern in the present situation, and matching with the DRAM operations should be explored sufficiently in the future.

There has been no systematic research reported on the correlation between the composition and electrical properties of PZT thin film aiming at its actual application in LSIs. This report introduces a practical metallo—organic chemical vapor deposition (MOCVD) method using a new source gas and the properties of PZT thin film with a wide range of composition fabricated by MOCVD, focusing on its applications in DRAMs.

2. MOCVD Method

To allow practical use of a material with a large number of component elements and with electrical properties strongly dependent on composition like PZT, what is most important is to develop a film deposition process which can easily achieve and control a wide range of composition, and the composition which seems to be best for device application should be found and determined

Figure 1. MOCVD-PZT Source Materials

among them. Such methods reported until now include sputtering, the sol-gel method and CVD. Among these, the sol-gel method is suitable for the evaluation of the material's solid-state properties because it allows any required composition according to the composition of the applied liquid, but it is not considered to be usable as manufacturing technology due to the difficulty in forming films with a controlled film thickness and deposition on various device topographies. It is believed that CVD can provide freedom of composition, but requires the greatest care in handling the source materials. Particularly with PZT, which has problems in the toxicity of source Pb and the low vapor pressure, the methods reported until now have not been practical for actual manufacturing technology. On this occasion, we selected the source materials shown in Figure 1 taking the coexistence of Pb source toxicity and vapor pressure into consideration.
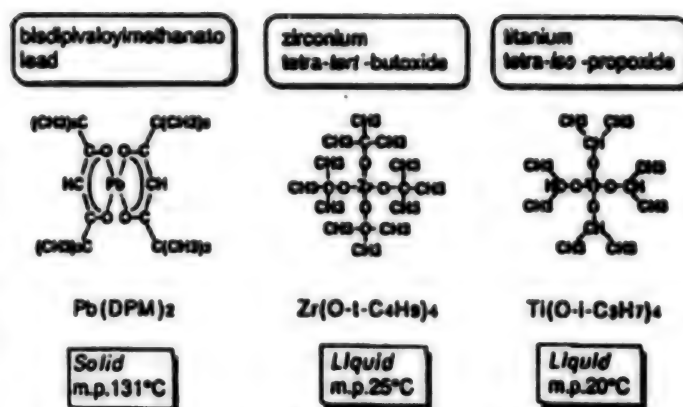
Substrate	Si(100), Pt(111), 6-inch ϕ Temp. = 600~700°C			
Source	$Pb(DPM)_2$	N_2 carrier	100~200 sccm	135°C
	$Zr(O-t-C_4H_9)_4$		0~100 sccm	30°C
	$Ti(O-i-C_3H_7)_4$		0~100 sccm	30°C
	O_2		700 sccm	
Pressure	1~2 Torr			
Depo. rate	5~20 nm/min			

Figure 2. Typical Condition of PZT-MOCVD

$Pb(DPM)_2$ (bisdipivaloylmethanato lead) is a beta-diketone complex of lead, and a nontoxic material which is a solid powder at room temperature. With a sufficiently low melting point compared to $PbCl_2$ and other materials previously used, it can be used to deposit thin films with satisfactory reproducibility and supply controllability by taking care to maintain the temperatures of the piping materials and reaction vessel walls. As Zr and Ti sources, $Zr(O-t-C_4H_9)_4$ (zirconium tetra-tert-butoxide) and $Ti(O-i-C_3H_7)$ (titanium tetra-iso-propoxide)

have been selected because they are non-toxic. We used sheet-type thermal CVD to fabricate PZT thin films on substrates under the typical conditions shown in Figure 2. The PZT is formed by the thermal oxidation by oxygen in the mixed gas of the above sources which is carried by carrier N_2. Si(100) and Pt(111) were used as substrates. Figure 3 shows the results of crystal structure evaluation made by X-ray diffraction of CVD-PZT of the as-depo state.
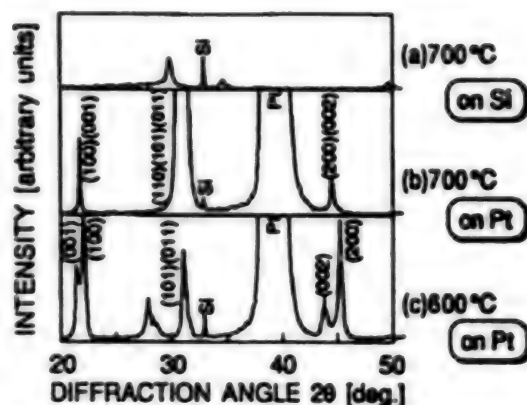

Figure 3. Crystallinity Evaluation by XRD (700°C, as-depo)

Although this figure shows some difference depending on the deposition temperature (the compositions may also be involved in the differences in crystal structure observed here because the compositions also vary under the same source supply condition depending on the deposition temperatures), it also shows that the Perovskite structure, which is the main factor causing the high relative dielectric constant, is not obtained on Si but obtained only on Pt as with sputtering and sol-gel methods.

What we should note here is that the Perovskite structure is not obtained through thermal treatment after film deposition, but obtained in the as-depo state. this has an important significance in application to thin films as described later. Figure 4 shows the scanning-type ion microscope (SIMS) element profiles in the film thickness direction of Pt/PZT/Pt structures fabricated by various film fabrication methods. With the sol-
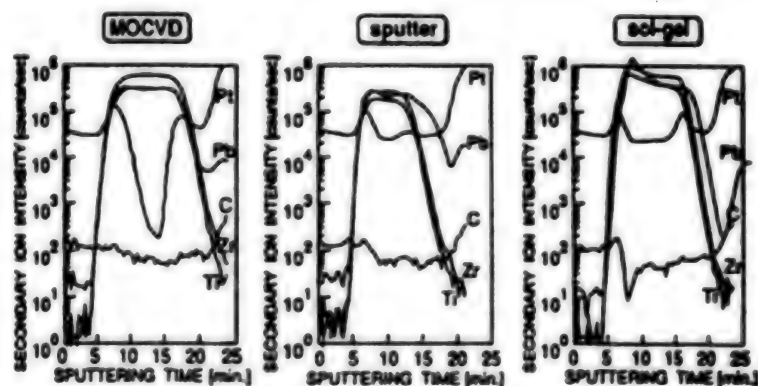

Figure 4. Comparison of Element Profiles of Various Film Fabrication Methods
(MOCVD: 700°C, as-depo.; Sputtering/sol-gel: 700°C, in O_2, thermal treatment for 20 min.)

gel and (low-temperature) sputtering methods, thermal treatment is required after film fabrication to cause Perovskite crystallization, and the solid-state reaction occurring during it seems to have caused the penetrations of substrate Pt into the PZT.

On the other hand, with CVD-PZT, the penetration of Pt is very small (although its deposition temperature of 700°C is the same as the thermal treatment temperature of 700°C of sol-gel/sputtered PZT). As the amount of Pt penetration is regarded as one of the determining factors of the withstand voltage (leakage current) of thin films, the results shown in Figure 4 indicate the necessity of implementing a Perovskite structure by vapor growth. In this

43

context, it can also be understood that high-temperature sputtering (in which the substrate is heated during sputter-deposition) is the recommended sputtering method. Additionally, even with CVD-PZT, if thermal treatment at a higher temperature than the deposition temperature is intentionally applied after film deposition, Pt penetration and the sudden increase of leak current accompanying it are confirmed, thereby indicating the need to consider the processing temperature in post process before its actual application in devices. Therefore, the optimum structure of a DRAM may be the "embedded bit line structure" shown in Figure 5, with which high-temperature heat treatment is not required after the formation of capacitors.
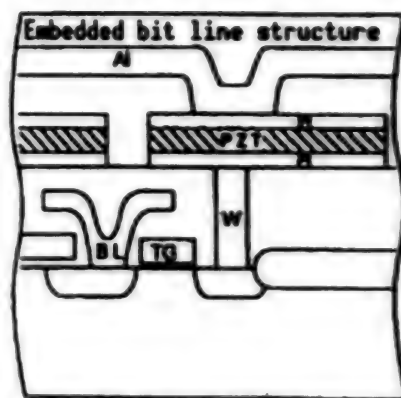

Figure 5. Example of Perovskite DRAM

As for the problems in MOCVD which are the mixture of carbon in the film due to the use of organic source materials and the resulting withstand voltage decrease, Figure 4 shows that the carbon content in the MOCVD-PZT is not different from the carbon in the upper Pt and sputtered PZT (which are deposited carbon-free). Since one of the motives to use PZT is the implementation of perfectly-plane stacked capacitors as described before, the coating performance of irregularities cannot be considered to be a definite advantage, but it is still confirmed that the PZT deposited by the present MOCVD method has a suitable coating performance.

3. Application in DRAM

The first thing to be considered in the application of PZT in DRAMs is how to handle the leakage current and ferro-electricity. Considering the throughput in film deposition, post-processing and the balance with the thicknesses of other films making up the memory cell, it may be more advantageous to secure the required capacitance by making the PZT film thinner with a composition providing small leakage current while compromising the relative

Figure 6. Effective Charge of Ferroelectric Capacitor in DRAM Operation

dielectric constant, rather than to form capacitors with a thicker PZT film with a composition providing a large relative dielectric constant and large leakage current.
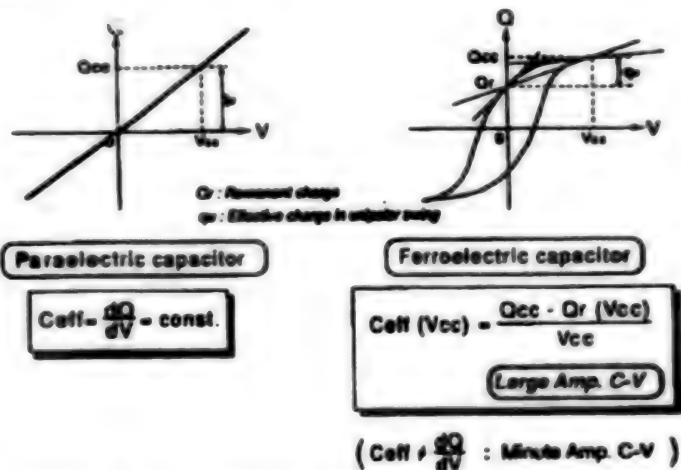
Figure 6 shows the relationship between the stored charges and pole plate voltages of metal injection molding (MIM) capacitors formed from paraelectric thin films and ferroelectric thin films. With the paraelectric capacitor, the

44

capacitor obtained by C–V measurement represents the gradient of the Q–V line, directly expressing the effective charge contributing to DRAM operation.

In this case, the effective charge is identical regardless of the unipolar swing (between $0 \leftrightarrow V_{cc}$) or the bipolar swing (between $-1/2\ V_{cc} \leftrightarrow 1/2\ V_{cc}$), and the modulation amplitude during C–V measurement has no influence.

On the other hand, with the ferroelectric capacitor, the capacitance obtained by ordinary minute–amplitude C–V measurement simply shows the gradient of the tangent of the Q–V hysteresis loop, and does not express the effective charge during DRAM operation. With a unipolar swing, the capacitor efficiency drops because of the presence of remanent charge Q_r.

The effective charge is obtained by subtracting Q_r from Q_{cc} (the charge induced on the pole plate when V_{cc} is applied), and the effective capacitance is obtained by dividing this by V_{cc}. Specifically, in Figure 6, it is represented by the gradient of the line connecting Q_{cc} and Q_r, and its value is smaller than the apparent capacitance obtained by minute–amplitude C–V measurement. The C–V measurement should therefore be performed using the same modulation amplitude as the DC bias voltage $(1/2)\ V_{cc}$ (which results in the variation of the amplitude following the DC bias sweep). The bipolar swing is not expected to present a drop in efficiency due to remanent polarization, but to be adversely influenced by problems of the transitory but large polarization reversal current and film fatigue. Based on the above studies, we decided the basic policy in the search for the composition of PZT for DRAM, which is to use a thin film with as small a remanent polarization and leakage current as possible in the unipolar swing mode.

As for the composition search process, we determined the following procedure after the studies of the Perovskite crystal model: First, the supply rate of the Pb source should be varied while maintaining the supply rates of the Zr ad Ti sources constant (ratio of 1:1 with respect to the flow of carrier N_2). After determining the Pb source supply rate which can provide a stable, low-leakage current, the ratio between the supply rates of the Zr and Ti sources is varied to search for the composition which can provide the lowest leakage current. The oxygen flow is set sufficiently high. For the evaluation of the electrical properties, after having deposited CVD–PZT thin films of about 2,500 Å with various compositions, Pt with a diameter of 1 mm was formed to allow evaluation based on the Pt/PZT/Pt capacitor structures. The items evaluated were J–V (leakage current density versus DC voltage), C–V and D–E (using a Sawyer (phonetic) tower circuit).

Figure 7 shows the results of these evaluations. The graphs show that the present CVD method makes it possible to obtain a wide range of compositions easily by controlling the source supply rates, and that the electrical properties are strongly dependent on the compositions. Namely, they show that PZT with a low leakage and weak ferroelectricity can be obtained when the relative content of Zr is increased while restricting Pb and Ti. With each composition, the leakage current when a voltage is applied to a virgin sample is always larger the first time than the second and later times, and the leakages of the second time and later are always identical (provided that the
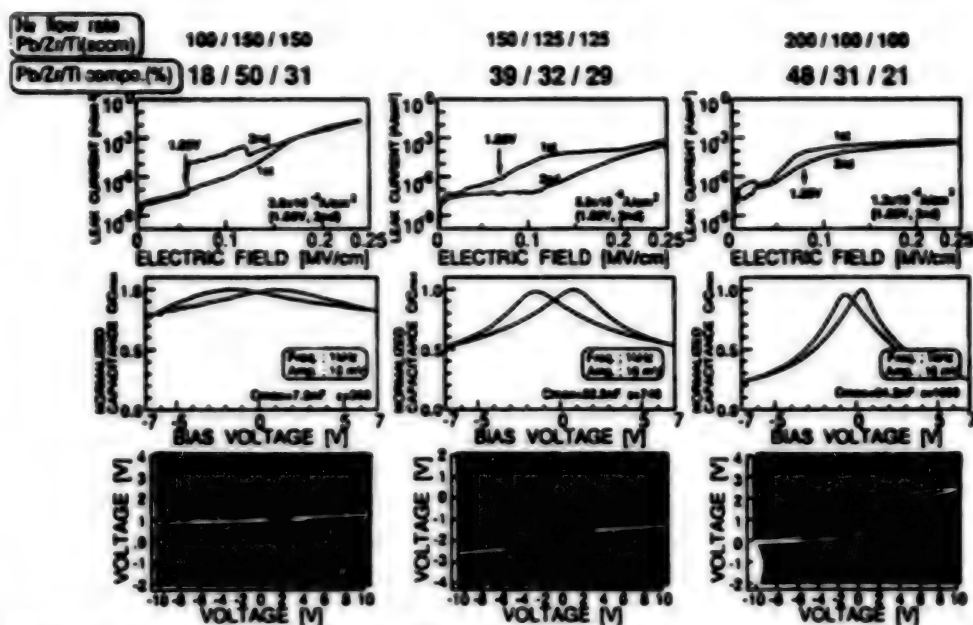
45

Figure 7(a). Electrical Property Changes According to Composition (Dependence on Pb source supply amounts)
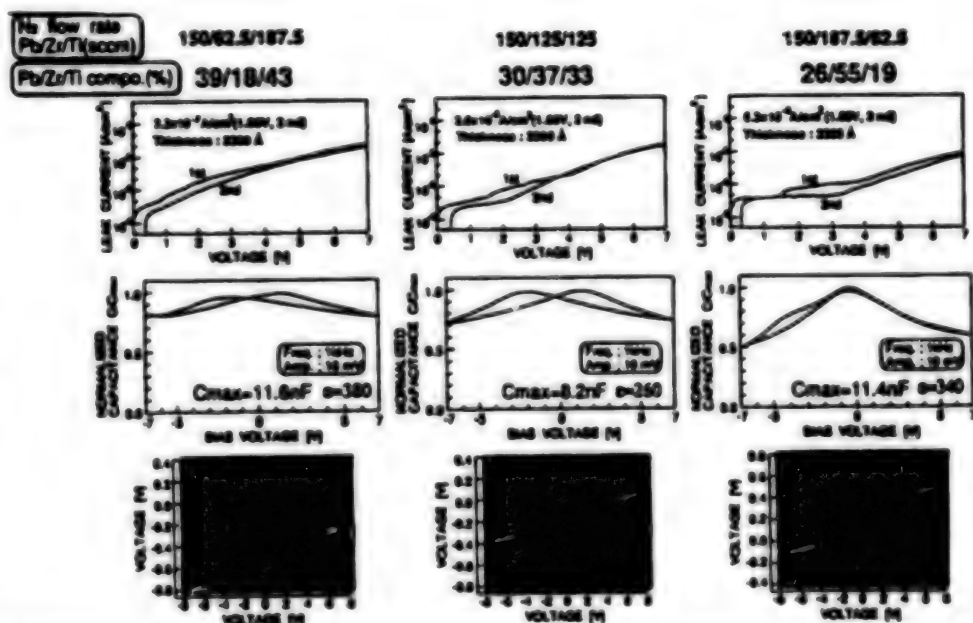

Figure 7(b). Electrical Property Changes According to Composition (Dependence on Zr source:Ti source supply ratio)

maximum voltage applied and polarity remain the same). Figure 7 also shows the C-V curves (together with the hysteresis of the bias voltage sweep direction) measured at minute amplitudes, and the relative dielectric constants (at the zero-volt bias point) calculated from them. As described above, these values

46

do not express the effective dielectric constant during unipolar-swing operations of DRAMs. The effective dielectric constants calculated from the capacitances measured by making the DC bias voltages and modulation amplitudes identical during unipolar-swing operations are shown in Figure 8.

What should be noticed in Figure 8 is that the maximum value of effective dielectric constant exists at specific bias voltages. This is thought to be due to the nonlinearity of the remanent polarization at the maximum applied voltage or to the dissimilarity of the hysteresis loop shapes. In Figure 8, it is shown that the composition particularly rich in Zr is paraelectric with small amplitude swings and is suitable for use in DRAM capacitors.

Figure 9 shows the influence of the history of voltage applications with polarity reversals on the leakage current. The figure shows that an increase of leakage current accompanying the polarity reversal is also observed with Zr-rich composition, confirming that the unipolar swing operation is desirable for the stabilization of leakage current.

Thickness of PZT :2300Å

Figure 8. Effective Relative Dielectric Constants in DRAM Operation (Dependence on swing amplitude)

Figure 10 shows the fatigue characteristics of the effective dielectric constants and leakage currents after the application of unipolar and bipolar stresses up to about 10^9 times. As the figure does not show any clear tendency, experiments with more stress repetitions may be required in the future. Figure 11 shows the relationship between the PZT thin film thickness, the leakage current density (at
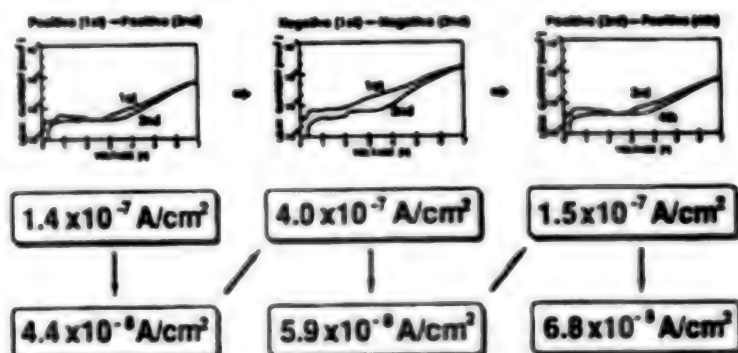
Figure 9. Influence of History of Voltage Applications on Leakage Current

the second unipolar swing) and the equivalent film thickness when converted into silicon oxide film thickness (effective value in DRAM operation). A characteristic of $T_{eq} - 10$ A and $J_t - 10^{-7}$A/cm^2 or less is required at the 256M DRAM level, and improvements will be required by fine-adjusting the composition and optimizing the deposition condition in the future.
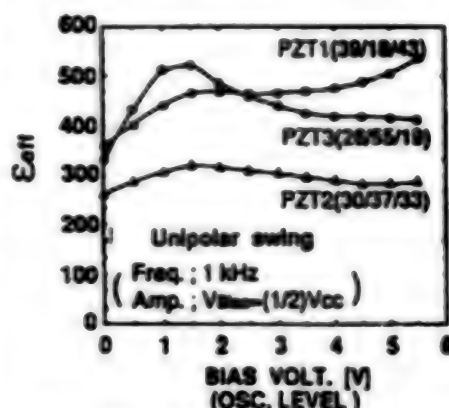
47

4. Conclusion

Now that easy-to-handle source materials for CVD have become available, the relationship between the wide range of PZT compositions and the electrical properties can be identified more easily and more quickly than before. As the use of CVD has made possible high-speed deposition of films as well as accurate control of film deposition recipes, for example, the setting of composition distribution in the film thickness direction and the management of initial nucleation, it is also expected that the controllability of the electrode interface structure and the crystal grains and grain boundary structure of polycrystalline Perovskite PZT can be improved by CVD. The dielectric substances for use in DRAM capacitors used to be limited to amorphous materials, and the introduction of polycrystalline materials such as PZT may necessitate taking the grain diameter and structure into consideration from the viewpoint of the prevention of dispersion of properties between minute memory cells. Also, it is easily predictable that there is a certain relationship between the grain structure and ferroelectricity or paraelectricity. The authors believe that future research into the PZT thin films for use in DRAM should be made from the structural aspect as well as from the compositional aspect. Besides, from the viewpoint of mass-production technology, it is also important to search for easy-to-handle $Pb(DPM)_2$ dielectric substance with a lower melting point, and to develop a manufacturing system which can improve the composition control and reproduction accuracy based on a direct control of the supplies of all source materials using a mass flow controller.
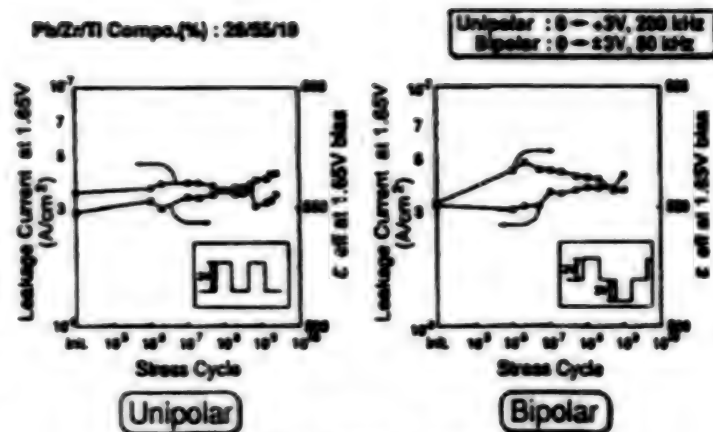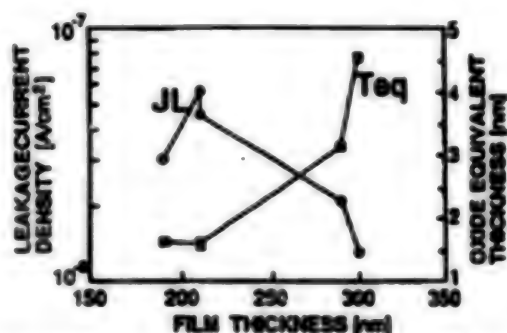

Figure 10. Fatigue Characteristics

Figure 11. Equivalent Film Thickness When Converted Into Silicon Oxide Film Thickness (Dependence on CVD-PZT Film Thickness)

Properties of SrTiO$_3$-BaTiO$_3$ Thin Film Fabricated by Sputtering Method, Application

[Article by Yoichi Miyasaka, Fundamental Research Laboratories, NEC Corp.]

[Text] 1. Introduction

The applications of ferroelectric thin films in LSIs can be divided into the implementation of nonvolatile memories based on spontaneous polarization switching and their utilization as dielectric thin films in the capacitors of DRAM cells. As research in recent years is mainly targeted at applications in nonvolatile memory devices, many recent reports deal with fabrication of thin films from ferroelectric substances which are in the ferroelectric phase under room temperature, for example PZT or Bi$_4$Ti$_3$O$_{12}$. On the other hand, from the viewpoint of dielectric thin film, materials which are in the paraelectric phase at room temperature (that is, materials with lower curie points than room temperature) can also be examined, so the range of material selection from a large number of known ferroelectric substances is rather wide. In this lecture, I will report on the results of our examinations of the film fabrication of SrTiO$_3$, BaTiO$_3$ and their solid solutions, (Ba,Sr)TiO$_3$, by means of sputtering methods in a broader meaning of the term, that is, including ion beam sputtering.

There have been many reports on the fabrication of BaTiO$_3$ thin films over a number of years.[1] We think there are fewer reports on SrTiO$_3$, but there is a fairly detailed report by Pennebaker.[2] Nevertheless, the film thicknesses dealt with in these previous reports are large compared to the level required for today's VLSI capacitors, and we have to study what kinds of properties can be obtained with thinner films. Besides, there are few reports on the dielectric characteristic of (Ba,Sr)TiO$_3$ thin films.

In the following, I will first report on the results of studies of thin films sputtered using these materials, then on the results of actual fabrication of SrTiO$_3$ film by ion beam sputtering (IBS). I will also report studies, made with SrTiO$_3$ thin film, on electrodes when the film is fabricated on Si.

2. Fabrication of $SrTiO_3$, $BaTiO_3$, and $(Ba,Sr)TiO_3$ Films by Sputtering Method

The results described in the following were obtained in film fabrication by RF magnetron sputtering.[3] The typical sputtering condition was an atmosphere of $Ar:O_2 - 9:1$, a sputtering pressure of 10 m Torr, and film thicknesses of 400-500 nm. The sputtering targets were prepared by pressing the sintered powder with the same composition as the desired film composition. The formation of thin films with the same compositions as the targets was confirmed by means of inductively coupled plasma (ICP) and electron probe microanalyzer (EPMA).

To investigate the basic properties, we fabricated a dielectric film on a Pd electrode (DC sputtered film with a thickness of 500 nm) on a sapphire substrate, and all of the following results were obtained using this kind of substrate. Many of the previous reports use Pt as the lower electrode, but we use Pd because our experience has shown that it has better adhesion to the substrate. The surface of the Pd film is slightly oxidized during dielectric thin film deposition at around 500°C or above, but this does not cause a problem because the Pd oxide is known to be electroconductive, which we also confirmed by ourselves. Also, as the $SiO_2(/Si)$ substrate may cause electrode separation due to the small coefficient of expansion, we decided to use sapphire substrates with a larger coefficient of expansion in order to make the basic experiments effective.

The electrical properties were measured by forming an Au/Ti upper electrode of 0.3 x 0.3 mm^2 on the dielectric thin film. With all samples dealt with in this report, we measured the capacitances from 100 Hz to 1 MHz, and confirmed that there were few cases of frequency dependence. However, strictly speaking, a very slight drop in capacitance occurs as the frequency is increased, so we use the values at 10 kHz for the dielectric constant and capacitance data in the following.

Figure 1 shows the relationship between the substrate temperatures and dielectric constants during deposition of $SrTiO_3$ and $BaTiO_3$ thin films. The figure shows that $SrTiO_3$ can provide a higher dielectric constant when compared at the same temperatures below 550°C, Figure 2 shows the changes with temperature of the capacitance and tan δ of $SrTiO_3$. Except for the sample with the lowest dielectric constant, this figure shows negative temperature coefficients similar to bulk materi-

Figure 1. Relationship Between Substrate Temperature and Dielectric Constant of $SrTiO_3$ and $BaTiO_3$

als, and the changes due to temperature increase as the dielectric constant increases. We also measured them with $BaTiO_3$ up to 220°C, but no dielectric anomalies were observed with any sample.
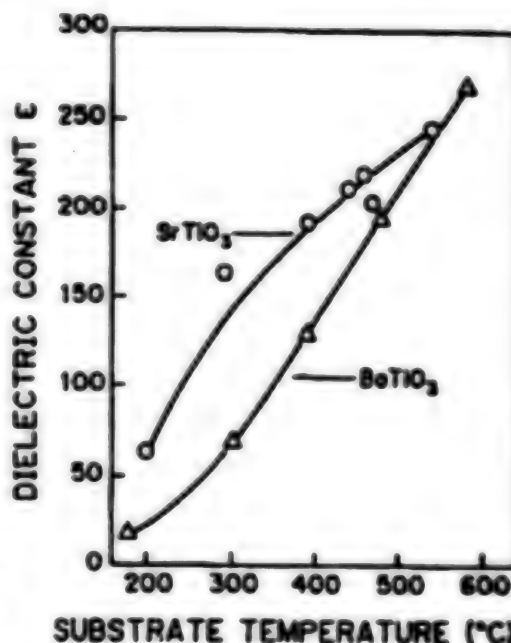
50
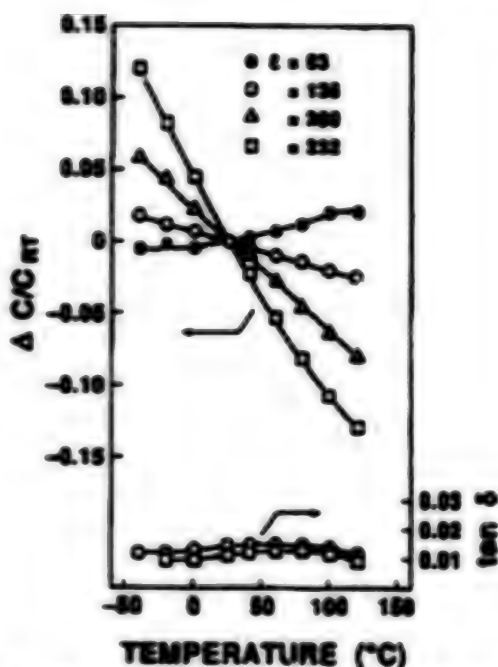
Figure 2. Changes of Capacitances and tan δ of SrTiO₃ Films With Temperature

Figure 3. Changes of Dielectric Constants of $(Ba_{1-x}Sr_x)$ TiO₃ Films According to Composition

Figure 4. Film Thickness Dependence of Dielectric Constant of $(Ba_{0.5}Sr_{0.5})TiO_3$ Film (deposited at 600°C)

Also, as reported in previous reports, the BaTiO₃ film has a pseudo-cubic crystal structure unless it is fabricated at a high temperature around 1,000°C or is subjected to thermal treatment, and no dielectricity anomalies have been observed, as in our results.

The experiments on (Ba,Sr)TiO₃ were made by varying the ratio of Ba and Sr as well as the target powder sintering temperature (800, 900, 1,000 and 1,100°C). The following description assumes their compositions can be expressed by the formula $(Ba_{1-x}Sr)TiO_3$. In this case, films with almost the same compositions as target powders can be deposited regardless of the value of x. The fact that higher substrate temperatures can provide larger dielectric constants also applied here like SrTiO₃, but it was also found that the dielectric constants obtained at high temperatures are dependent on the composition (value of x) as it can be expected from the characteristic of the bulk material, and that they are also largely dependent on the target powder sintering temperature. Figure 4 shows the results obtained with a sample deposited with a substrate temperature of 600°C. The results obtained with the powder target sintered at 1,100°C were almost the same as those obtained with powder sintered at 1,000°C.

As shown in Figure 3, the dielectric constant is maximum near the composition of x = 0.5, that is, the composition in which the contents of Ba and Sr are
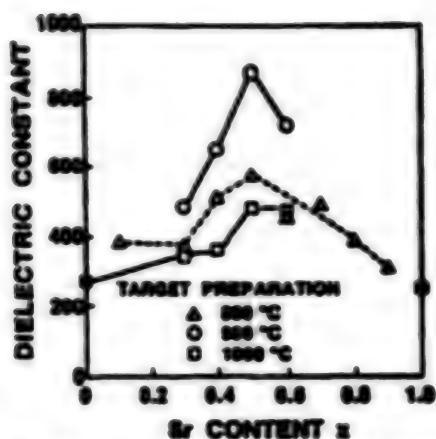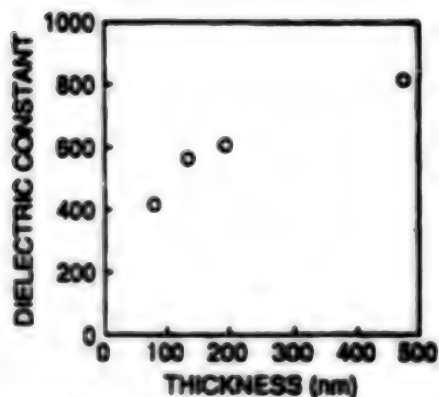
51

equal, regardless of the powder target used. While the previous report on the composition dependence of bulk ceramics[4] leads to an analogical inference that the dielectric constant at room temperature is maximum with x - 0.3~0.6, the maximum points in our results obtained with thin films are shifted to the Sr-rich side. From Figure 1, the reason for this can be considered to be as follows: Considering that the dielectric constants of bulk ceramics are 300 with $SrTiO_3$ and 1,200 with $BaTiO_3$, the results in Figure 1 suggest that $SrTiO_3$ can provide a thin film with a closer crystal structure to the bulk ceramic. If we draw an analogy from this, the compositions closer to $SrTiO_3$ may provide a closer crystal structure to bulk ceramic, and the synergistic effect of this fact and the original composition dependence of the bulk ceramic may have achieved a compositional dependence as shown in Figure 3. With Figure 3, when powder target sintered at 900°C is used, the maximum dielectric constant near 900 was obtained with x - 0.5. Even with a film with x - 0.5, fabricated using target sintered at 800°C, an increased dielectric constant near 900 was obtained after thermal treatment at 700°C or more. The dependence on the target is thought to be due to the differences in the states, such as energy states, of sputtered particles. We hope to clarify its cause by means of plasma spectroscopic analysis.

The changes with temperature of dielectric constants showed generally negative temperature coefficients as far as we investigated them in the range of x < 0.5, but a peak which is very broad but seems to indicate a dielectric anomaly is observed at around -10°C only with films with dielectric constants of more than 800.

Figure 4 shows the film thickness dependence of the dielectric constant of a film with x - 0.5, deposited using a target sintered at 900°C. The figure shows a gradual drop in the dielectric constant following the decrease of film thickness, and the dielectric constant is between 400~500 at about 100 nm. As a dielectric constant of 200 is obtained with $SrTiO_3$ film of 50 nm as described later, the present characteristics of the two materials can be regarded as similar from the viewpoint of capacitance. However, from the viewpoint of the bulk characteristics, a higher dielectric constant can be expected from $BaTiO_3$. We also hope to improve it further by improving the film fabrication method.

3. Fabrication of $SrTiO_3$ Film by Ion Beam Sputtering (IBS)

$SrTiO_3$ thin films fabricated by RF magnetron sputtering present large variations in leakage current if the film thickness is less than 100 nm, so we studied the possibility of film fabrication by IBS as a technique to improve this.[5] IBS is a flexible method compared to ordinary sputtering methods because it can handle the process where the target is sputtered and the process where the target is deposited on the substrate separately. The substrates and characteristic measuring techniques used were the same as those described in the previous section.

The targets were also prepared by pressing $SrTiO_3$ powder. Sputtering was performed by bombarding Ar ions from a Kaufman ion gun, and O_2 gas was introduced around the substrate. the total pressure during film fabrication was between 1.2 and 2.2 x 10^{-4} Torr (the minimum value being the partial

pressure of Ar alone). Films fabricated without introducing O_2 were electrocon-
ductive due to the lack of oxygen, but insulating films could be fabricated by
introducing O_2 gas with a partial pressure of 2×10^{-5} Torr or more. Similar
to the sputtering methods described previously, the compositions of the target
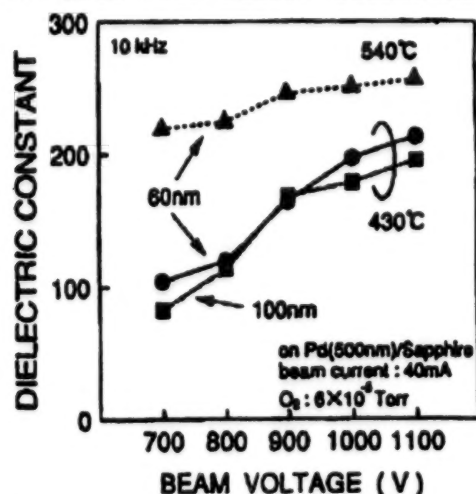and film were almost identical, that is, Sr/Ti up to 1.

Figure 5. Beam Voltage Depen-
dence of Dielectric Constant
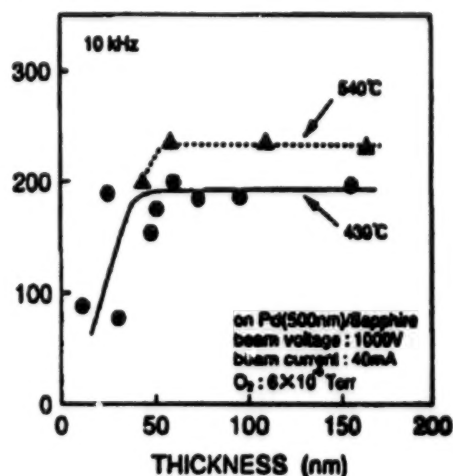of IBS–SrTiO₃ Film

Figure 6. Film Thickness Depen-
dence of Dielectric Constant of
IBS–SrTiO₃ Film

As shown in Figure 5, the results obtained show that the dielectric constant
is fairly dependent on beam voltage. This dependence is more noticeable with
lower substrate temperatures. On the other hand, the results show little
dependence on the beam current (which affects the film fabrication speed), so
it can be considered that the beam voltage dependence of the dielectric
constant may be explained from the beam voltage dependence of the sputtered
ions. The relation between the substrate and dielectric constant when film is
fabricated with a beam voltage of 1,000 V was almost the same as the case of
the sputtering method described in the previous section.

Figure 6 shows the film thickness dependence
of the dielectric constant. The dielectric
constant is constant with film thicknesses
above 50 nm, but it tends to drop with film
thicknesses below 50 nm. Figure 7 shows the
current–versus–voltage characteristic of a
53–nm film fabricated with a substrate
temperature of 540°C. The current density
may be sufficient to be practical, with no
more than 10^{-8}A/cm² up to 2 V. As shown in
Figure 6, this film has a dielectric con-
stant of 230 and properties capable of
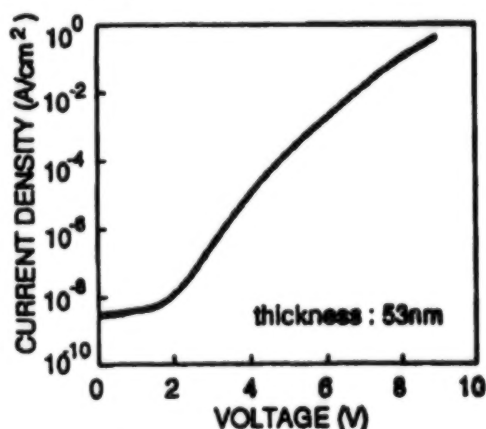implementing a capacitance density of 38
fF/μm² with a planar design.

Figure 7. Current–Vs–Voltage
Characteristics of IBS–SrTiO₃
Film

Although rigorous discussion is not possible before plasma spectroscopy and other analyses, IBS can be considered as being capable of providing good insulation from even thin films of about 50 nm thanks to smaller plasma damage than in ordinary sputtering.

4. Lower Electrode in Film Fabrication on Si

With the cell capacitors in DRAMs, the lower electrode (storage node) should be connected to the transistor, so we must assume the presence of Si below the lower electrode. The previous design was ideal because its lower electrode is made of Si itself. However, if this design is used with an oxide such as a ferroelectric substance, the Si surface would be oxidized during fabrication and SiO_2 would be generated, which would greatly reduce the effective dielectric constant[6] making it impossible to utilize the high dielectric constant.

According to our studies made on various materials, the most effective design of the lower electrode is a two-layer structure of Pt/Ta or Pt/Ti.[7] In case $SrTiO_3$ is formed directly on Si or in case only Pt is formed on Si then $SrTiO_3$ is formed on it, the effective dielectric constant (= measured dielectric constant) decreases as the film thickness decreases as shown in Figure 8. With Pt/Si, as a process of silicide generation → SiO_2 generation progresses during $SrTiO_3$ film fabrication, the result has been confirmed to be no different from the case of direct formation on Si. Ta and Ti function as a barrier against dispersion between Pt and Si and, as a result, high dielectric constants are observed with Pt/Ta and Pt/Ti as shown in Figure 8. It has also been confirmed that Pt/Ta is more effective up to higher temperatures.

Figure 8. Effective Dielectric Constants of $SrTiO_3$ Films Fabricated Directly on Si and Metallic Film Formed on Si

5. Conclusion, Future Prospects

In the above, we have stated that a dielectric constant of around 200 can be obtained with $SrTiO_3$ thin film fabricated by sputtering, and an even higher dielectric constant can be expected with $(Ba,Sr)TiO_3$ having a composition with a Ba/Sr ratio near 1. As for $SrTiO_3$, we could obtain a good insulation characteristic with a 50-nm thick film fabricated by IBS. With $(Ba,Sr)TiO_3$, significant superiority over $SrTiO_3$ is not found because the dielectric constant is, for the present, highly dependent on film thickness, but we hope to exhibit its potential by future studies.

With the materials dealt with in this report, the target compositions are reflected in the thin film compositions almost uniformly. Therefore, at least
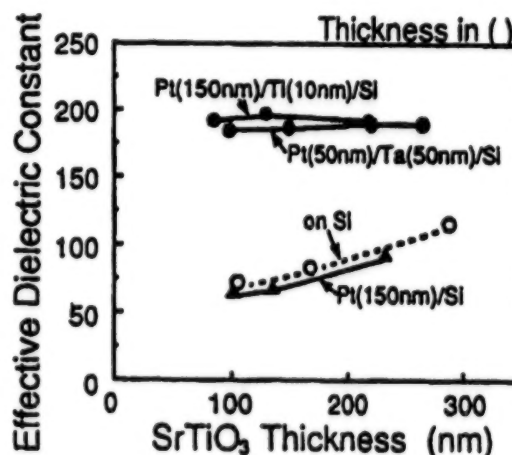
with regard to sputtering methods, film fabrication is very easy compared to Pb or Bi type materials, which is one of the great advantages of these materials.

Recently, NEC fabricated a prototype capacitor with a size usable in a 64M DRAM, using $(Ba,Sr)TiO_3$ thin film and Pt/Ta/Si structure electrodes.[8] But there are still many problems to be overcome, for example, the increase of capacitance density by improving the dielectric film properties, further studies of electrode materials and the development of processing technologies. From the viewpoint of covering steps and irregularities, CVD film deposition is ideal if it becomes feasible.

References

1.   Pratt, I.H., PROC. IEEE 59, 1971, p 1440.

2.   Pennebaker, W.B., IBM J. RES. DEVELOP., November 1969, p 686.

3.   Miyasaka, Y., et al., Proc. 7th Int. Symp. Applications of Ferroelectrics 1990, in press.

4.   Hellwege, K.H., et al., Eds., Landolt–Bornstein III/16a (Ferroelectric Oxides), 1981, p 416.

5.   Yamamichi, S., et al., JPN. J. APPL. PHYS., Vol 30, 1991, p 2193.

6.   Matsubara, S., et al., MAT. RES. SOC. SYMP. PROC., Vol 200, 1990, p 243.

7.   Sakuma, T., et al., APPL. PHYS. LETT., Vol 57, 1990, p 2431.

8.   Koyama, K., et al., 1991 IEDM.

– END –

END OF
FICHE

DATE FILMED

6 Nov 1992